Loss of ABAP1 INTERACTING PROTEIN 10 (AIP10) enhances colonization by beneficial bacteria in the native root microbiome and following bioinoculant application in *Arabidopsis thaliana*

Maria Clara de Oliveira Urquiaga[1±], Helkin Giovani Forero Ballesteros[1,2±], João Victor Silva[1], Patrícia Montessoro[1,2], Sara Gawantka Evangelista[1], Adriana Silva Hemerly[1*]

1- Laboratório de Biologia Molecular de Plantas, Instituto de Bioquímica Médica Leopoldo de Meis, Universidade Federal do Rio de Janeiro, Rio de Janeiro, RJ, Brazil
2- Hapiseeds Pesquisa e Desenvolvimento LTDA, Rio de Janeiro, RJ, Brazil (Present address)

± These authors have contributed equally to this work and share first authorship.
* Author for correspondence: hemerly.adriana@gmail.com

Email address for each author:

1. Maria Clara de Oliveira Urquiaga: mariaclara.urquiaga@gmail.com (ORCID: 0000-0001-9539-6543)
2. Helkin Giovani F. Ballesteros: helfos85@gmail.com (ORCID: 0000-0001-5365-1841)
3. João Victor Silva de Oliveira: jvsilvaolivera.2001@gmail.com (ORCID: 0009-0000-4657-0242)
4. Patricia Montessoro: patriciamontessoro@gmail.com (ORCID:0000-0001-7541-7714)
5. Sara Gawantka Evangelista: saragawantka@gmail.com (ORCID:0009-0008-9133-5856)
6. Adriana S. Hemerly: hemerly.adriana@gmail.com (ORCID: 0000-0003-3748-7118)

Submission date: 25/01/2026
Number of tables: 0
Number of figures: 9
Supplementary data: 6 figures and 2 tables

Abstract

Sustaining high agricultural productivity with minimal environmental impact requires innovative and sustainable strategies that reduce reliance on mineral fertilizers. To enhance root colonization by plant growth-promoting bacteria (PGPB), either within the native microbiome or through bioinoculant application, represents a promising strategy to improve crop performance while reducing mineral fertilizer use. However, their effectiveness largely depends on plant genetic factors that regulate microbial recruitment and colonization. Here, we tested whether silencing the ABAP1 Interacting Protein (AIP10), a negative regulator that links cell division with primary metabolism, modulates the association of Arabidopsis thaliana to PGPB. Transcriptome profiling of aip10-1 knockout mutant revealed extensive reprogramming of metabolic pathways associated with plant-microbe interactions. Bacterial community composition was reshaped in aip10-1 root microbiome, favoring the association with specific plant growth-promoting taxa. Under low fertilization, aip10-1 plants showed enhanced responsiveness to bioinoculants, with increased biomass accumulation and reproductive performance. These effects were accompanied by modulation of plant nitrogen uptake and assimilation pathways, including genes involved in nitrate transport and ammonium incorporation, together with increased bacterial colonization. Finally, we propose that AIP10 acts as a regulatory node coordinating growth, metabolism, and microbial recruitment, thereby contributing to improved plant performance and functional integration with beneficial bacteria.

Keywords: beneficial association, nitrogen, biological nitrogen fixation, cell cycle regulator, microbiome, ABAP1

1. Introduction

Global population growth has increased the demand for agricultural products, including food, bioenergy, and other bioproducts, while climate change negatively impacts agricultural productivity. To sustain high yields while protecting the environment, modern agriculture must develop innovative and sustainable technologies that reduce environmental impacts, particularly those associated with the excessive use of chemical fertilizers, which contribute to increased greenhouse gas (GHG) emissions (Tilman et al., 2011). In parallel, nitrogen use efficiency (NUE) is estimated to remain below 50% for many crop species (Mueller et al., 2019; Govindasamy et al., 2023). Bioinoculants based on non-nodulating Plant Growth Promoting Bacteria (PGPB) represent a sustainable alternative to mineral fertilization, as they increase nutrients availability, improving soil fertility mainly through biological nitrogen fixation (BNF) and phosphate solubilization (Carvalho et al., 2016; Omara et al., 2019; Zuluaga et al., 2020; Favero et al., 2021; Pereira et al., 2021; Rodrigues et al., 2022; Galindo et al., 2024). Furthermore, PGPB can stimulate plant development by synthesizing phytohormones, modulating antioxidant production, and altering the expression of defense-related genes, thereby enhancing plant tolerance to both biotic and abiotic stresses (Vargas *et al.*, 2014; Fukami *et al.*, 2017; Filgueiras *et al.*, 2020; Moretti *et al.*, 2021; Nunes *et al.*, 2021; Orozco-Mosqueda *et al.*, 2023).

Agriculturally important non-nodulating monocot crops, such as maize, rice and sugarcane have shown beneficial responses to inoculation with bioinoculants based on non-nodulating diazotrophic bacteria (Hardoim et al., 2020; Pankievicz et al., 2021; Carvalho et al., 2022; Ferrarezi et al., 2022; Tian et al., 2022; Fonseca et al., 2025). Although FBN in these crops is less efficient than in legumes, numerous studies have demonstrated that bacterial inoculation significantly increases grain yield and biomass with BNF contributing up to 37% of the total nitrogen in maize (Alves *et al.*, 2014; Di Salvo *et al.*, 2018; dos Santos *et al.*, 2020; Aquino *et al.*, 2021; Dias *et al.*, 2021). The use of PGPB-based bioinoculants represents a promising strategy for developing more resilient and productive crops. However, their efficient application still faces major challenges. The success of these interactions depends on both biotic and abiotic environmental factors, as well as on the host plant genotype by modulation of plant gene expression (Carvalho *et al.*, 2011, 2014; Vargas *et al.*, 2012; Rosman *et al.*, 2024). This modulation allows the host plant to recognize the bacterial strain as a beneficial partner and, in turn, regulate plant gene expression to facilitate PGPB colonization, thereby directly or indirectly activating plant pathways that promote plant growth (Carvalho *et al.*, 2011; Do

Amaral *et al.*, 2014; Espindula *et al.*, 2019; Hardoim *et al.*, 2020; Ballesteros *et al.*, 2021; Pankievicz *et al.*, 2021; Thiebaut *et al.*, 2022; Rosman *et al.*, 2024).

Several studies have shown that alterations in plant genes can influence the assembly of root-associated bacterial communities, indicating that root microbiome composition is strongly shaped by plant genotype (Zang *et al.,* 2023). Modulation of defense-related pathways, such as salicylic acid signaling, has been reported to affect the recruitment of specific bacterial groups in the rhizosphere (Lebeis *et al.*, 2015). Likewise, genes involved in key signaling modules including the PHR1–RALF–FERONIA pathway have been implicated in shaping root-associated microbial communities with distinct functional capacities (Tang *et al.*, 2022). Additionally, genes regulating the production of root-derived metabolites, such as coumarins, contribute to differences in microbial composition and the enrichment of plant growth–promoting taxa (Stringlis *et al.*, 2018). Together, these studies highlight that genetic variation in plants, including reductions in gene activity, can play a significant role in determining the structure and function of the root microbiome.

Plant plasticity, which allows the modulation of plant growth in response to different environmental cues, including association with PGPB that enhance plant biomass and productivity. Ultimately, biomass increases are driven by higher rates the regulation of cell division rates (Qi and Zhang, 2020; Pierik *et al.*, 2021; Zluhan-Martínez *et al.*, 2021). Recently, our group described a novel cell cycle regulator, the ABAP1 Interacting Protein 10 (AIP10), which acts in a central hub integrating cell division rates with transcriptional reprogramming of basal metabolism (Montessoro *et al.*, 2025). This role is mediated by AIP10 protein interactions with the Armadillo BTB Arabidopsis protein 1 (ABAP1), a negative regulator of the cell cycle in plants, and with KIN10, a catalytic subunit of the Sucrose non-fermenting-1-related protein kinase 1 (SnRK1) (Masuda *et al.*, 2008; Montessoro *et al.*, 2025). In *Arabidopsis thaliana, aip10-1* knockout mutant plants exhibited increased cell division rates, resulting in enhanced shoot and root vegetative growth, as well as higher numbers of silique and seed production (Montessoro *et al.*, 2025). In addition, reduced *AIP10* expression triggered a major transcriptional reprogramming of plant primary metabolism mediated by SnRK1, leading to increased photosynthetic and water use efficiency and greater carbon fixation that met plant energy demands for increased biomass accumulation, and higher contents of proteins, lipids and carbohydrates (Montessoro *et al.*, 2025).

Developing strategies that enhance plant-bacteria interaction is a promising approach to increasing agricultural productivity and promoting more sustainable agriculture. *Arabidopsis thaliana* was already used as a model system to assess developmental responses and proteomic

141 changes triggered by association with PGPB, such as endophytic diazotrophic bacteria (Cohen
142 *et al.*, 2015; Souza *et al.*, 2016; Leandro *et al.*, 2019; Dos Santos *et al.*, 2020). Here, we
143 evaluated the role of *AIP10* in plant interactions with PGPB, both within the native root
144 microbiota and following inoculation with PGPB-based inoculants. The previously described
145 *A. thaliana aip10-1* full knockout mutant was used as a model and analyzed using
146 complementary approaches, including gene expression profiling by RT-qPCR and RNAseq
147 transcriptome data; root and soil microbiome characterization by metabarcoding; PGPB
148 inoculation followed by quantification and localization using confocal microscopy; and
149 comprehensive plant phenotyping. In this work, we showed that *AIP10* expression is
150 downregulated in sugarcane and in *A. thaliana* by successful PGPB colonization. The
151 transcriptional profile of *aip10-1* roots resembled signatures reported in genotypes with
152 enhanced capacity to interact with beneficial microorganisms. Loss of AIP10 function in *A.*
153 *thaliana* reshaped root-associated bacterial communities, promoting the recruitment of specific
154 beneficial PGPB species, while being depleted in potentially pathogenic taxa. Consistently,
155 *aip10-1* plants showed better colonization by the PGPB *Herbaspirillum seropedicae* and
156 *Gluconacetobacter diazotrophicus,* leading to increased vegetative and reproductive growth.
157 Moreover, *aip10-1* plants exhibited improved responses to bioinoculants under low fertilizer
158 conditions, accumulating biomass comparable to that of non-inoculated mutants grown under
159 high fertilizer input. Taken together, our findings suggest that silencing *AIP10* expression
160 represents a promising strategy to enhance PGPB colonization in the root microbiome or in
161 response to bioinoculants, and to improve nutrient use efficiency under reduced chemical
162 fertilization.
163

164 ## 2. Material and Methods

165 ### *2.1. Bacterial Strains and Growth Conditions*

166 For plant inoculation, the diazotrophic bacterial strain *Gluconacetobacter*
167 *diazotrophicus* PAL5 DsRed, labeled with red fluorescent protein and *Herbaspirillum*
168 *seropedicae* RAM10, labeled with green fluorescent protein, kindly provided by Dr. Gonçalo
169 Apolinário de Souza Filho (State University of Norte Fluminense Darcy Ribeiro), and
170 *Herbaspirillum seropedicae* HRC54 (BR 11335), obtained from EMBRAPA Agrobiologia
171 (Rio de Janeiro, Brazil), were used. Additionally, the commercial biofertilizer BioFree® (liquid
172 formulation), supplied by BioFROST and registered with the Brazilian Ministry of Agriculture,
173 Livestock and Food Supply (MAPA, No. PR001593-8.000001), containing *Azospirillum*

174 *brasilense* Ab-V6 and *Pseudomonas fluorescens* CCTB03 (1×10^{11} CFU/L), was employed in
175 the assays. *G. diazotrophicus* PAL5 DsRed was cultured in LGI-P medium (100 g/L granulated
176 sugar; 2 mL/L K_2HPO sol. 10%; 6mL/L KH_2PO_4 sol. 10%; 2 mL/L $MgSO_4.7H_2O$ sol. 10%; 2
177 mL/L $CaCl_2.2H_2O$ sol. 1%; 1 ml/L $FeCl_3.6H_2O$ sol. 1%; 2 mL/L $Na_2MoO_4.2H_2O$ sol. 0.1%; 5
178 mL/L bromothymol blue sol. 5% w/v in 0.2N KOH; pH 5.8) supplemented with streptomycin
179 (50 mg/L) and 1 mL of vitamin stock solution (biotin 100mg/L; pyridoxal-HCL 200 mg/L)
180 per liter of medium (Baldani *et al.*, 1996) and *H. seropedicae* HRC54 was grown in JNFB
181 medium (5 g/L malic acid; 6 mL/L K_2HPO sol. 10%; 18 mL/L KH_2PO_4 sol. 10%; 2 mL/L
182 $MgSO_4.7H_2O$ sol. 10%; 1 mL/L NaCl sol. 10%; 2 mL/L bromothymol blue sol. 5% w/v in
183 0.2N KOH; 4 mL/L FeEDTA sol. 1.64%; 4 g/L KOH; 1,07 g/L NH_4Cl; pH 6.0) supplemented
184 with 1 mL of vitamin stock solution and 2 mL of micronutrients stock solution (1 g/L
185 $Na_2MoO_4.2H_2O$; 1.175 g/L MnSO.HO; 1.4 g/L HBO; 0.04 g/L CuSO.5HO; 0.12 g/L
186 ZnSO.7HO) per liter (Baldani *et al.*, 1996). Both strains were subsequently transferred to
187 DYGS liquid medium (2 g/L malic acid; 2 g/L glucose; 1.5 g/L bacteriological peptone; 2 g/L
188 yeast extract; 0.5 g/L K_2HPO_4; 0.5 g/L $MgSO_4.7H_2O$ and 1.5 g/L glutamic acid, pH 6.0 for
189 HRC54 and pH 5.8 for Pal5 without malic acid) (Baldani *et al.*, 1996) and incubated at 30 °C
190 with agitation (200 rpm) for 6–12 hours until reaching an optical density at 660 nm of
191 approximately 0.8, corresponding to ~10^8 cells mL^{-1}. For plant inoculation, bacterial cultures
192 and the commercial inoculant were diluted 1:1000 (v/v) in autoclaved distilled water.

193 ***2.2. Plant material and inoculation with plant-growth promoting bacteria***

194 Seeds of the wild-type *Arabidopsis thaliana* ecotype Col-0 and the knockout mutant
195 line *aip10-1* (SALK_022332, T-DNA insertion), obtained from the Salk collection (Salk
196 Institute Genomic Analysis Laboratory) and previously characterized (Montessoro *et al.*,
197 2025), were used in association assays with diazotrophic bacteria. The seeds were sterilized by
198 exposure to chlorine gas, generated by the reaction between 97 mL of bleach (4.3%) and 3 mL
199 of hydrochloric acid (37%). After 2 hrs of treatment, the seeds were left in a laminar flow hood
200 until the gas had completely evaporated. Then, they were sown in Petri dishes containing
201 Murashige and Skoog (MS) ½ medium, supplemented with 0.05% 2-(N-morpholino)
202 ethanesulfonic acid (MES), 1% sucrose and 0.8% Phytagel (Sigma-Aldrich®), adjusted to pH
203 5.7. Seeds were stratified at 4 °C for 2 days and subsequently grown vertically in a growth
204 chamber with a 12/12 hrs photoperiod at 21 °C.

205 Four days after germination (4 DAG), 2 µL of the diluted bacterial suspension (1:1000),
206 containing approximately 10^2 cells μL^{-1}, were applied to the root zone. Control seedlings were
207 mock-treated with sterile DYGS medium diluted in the same proportion. After inoculation, the
208 seedlings were transferred to Petri dishes containing modified MS ½ medium (sucrose-free)
209 and maintained under the same culture conditions for another 7 days, totaling 11 DAG. For
210 molecular analyses, three biological replicates per treatment were harvested at 11 DAG, with
211 shoots and roots separated, frozen in liquid nitrogen, and stored at −80 °C. Plants were then
212 transplanted into pots containing a standard mixture of substate:vermiculite (3:1, w/w) and
213 grown under a 16/8 hrs photoperiod at 21 °C until 17 DAG.
214 Regarding the experiment with different nutritional doses, after a 6-day acclimatization
215 period, the plants were watered with two different concentrations of NPK 20-20-20 fertilizer,
216 with a final concentration of 0.06 g/L (low availability) and 0.12 g/L (high availability). The
217 plants were harvested at 31 DAI (35 DAG) for phenotypic analysis, and their productivity was
218 evaluated at 60 DAG.

219 ***2.3. Phenotypic analyses of A. thaliana plants***

220 Phenotypic analyses were performed on *A. thaliana* plants after separating shoots and
221 roots at 31 DAI. Fresh matter weight was measured using an analytical precision balance with
222 eight biological replicates. Thereafter, shoot and root samples were then placed in paper bags
223 and oven-dried at 60 °C for 6 days. Dry weight was subsequently measured using the same
224 balance, with eight biological replicates, to determine biomass. In addition, the rosette area was
225 determined from images evaluated in imageJ software (Schindelin *et al.*, 2012). The values of
226 fresh and dry matter and rosette area obtained were statistically analyzed using GraphPad Prism
227 software version 8.0.0. Statistical analysis was performed using Student's T-test. Statistical
228 significance was defined in all cases as p-value < 0.05
229 To analyze root development, harvested roots were immersed in 70% ethanol for 7
230 days. Subsequently, roots were laid out in an acrylic container (10 × 45 cm), with water at an
231 approximate depth of 1 cm for scanning. They were then characterized by image analysis using
232 WinRHIZO Pro® software (Regent Instruments, QC, Quebec, Canada) coupled to an Epson
233 Expression 11000XL LA2400 image scanner, as described in previous works (Bauhus and
234 Messier, 1999). Root length (cm) and surface area (m^2) were evaluated in five plants per
235 treatment. All analyzes used the Student's T-test. Statistical significance was defined as p-value
236 < 0.05.

237 Productivity analyses were performed at 56 DAI (60 DAG), including measurements
238 of number of siliques, length of the main inflorescence axis, and weight of seeds per plant. The
239 resulting data were subjected to statistical analysis using GraphPad Prism software version
240 8.0.0. Statistical significance was assessed using Student's T-test. The significance level of p
241 < 0.05 was used to determine statistical significance across all analyses.
242
243 ***2.4. Photosynthetic pigments***
244 Chlorophyll *a* and chlorophyll *b* were extracted at 31 DAI using dimethyl sulfoxide
245 (DMSO). Two rosette discs from the fifth leaf were incubated in 1 mL of DMSO for 72 h at
246 room temperature in the dark. Absorbance was measured at 480, 649.1, and 665.1 nm
247 (NanoDrop™ 2000), and pigment concentrations were calculated based on standard equations
248 ($Ca = 12.74 \times A665.1 - 3.62 \times A649.1$; $Cb = 25.06 \times A649.1 - 6.5 \times A665.1$). Results were
249 expressed as µg/g fresh weight. Statistical analysis was based on the Student's T-test for all
250 comparisons. Statistical significance was defined as p-value < 0.05.

251 ***2.5. RNA extraction and Real-time quantitative PCR***
252 For molecular analyses, plant roots were macerated in liquid nitrogen and immediately
253 stored at −80°C. At 11 DAG, total RNA was extracted from inoculated and non-inoculated
254 samples of each genotype using a lithium chloride–based protocol, as described by (Logemann
255 *et al.*, 1987). RNA concentration was determined with a NanoDrop™ 2000c spectrophotometer
256 (Thermo Scientific, USA), and its integrity was assessed by electrophoresis in a 1% agarose
257 gel stained with ethidium bromide. Approximately 5 µg of total RNA was treated with DNase
258 I (Biolabs), according to the manufacturer's instructions, and used for the synthesis of the first
259 strand of cDNA with GoScript reverse transcriptase (Promega). Gene expression analyses were
260 performed by RT-qPCR using SYBR Green PCR Master Mix (Applied Biosystems). Each
261 reaction was assembled in a final volume of 10 µL, containing 2 µL of cDNA diluted 1:3, 5 µL
262 of SYBR Green mix, 1 µL of each primer (forward and reverse, 10 µM) and 1 µL of sterile
263 ultrapure water. The primers specific for the target genes analyzed are listed in Table S1.
264 Expression normalization was performed based on the constitutive genes *UBIQUITIN 14*
265 (*UBI14*) and *GLYCERALDEHYDE-3-PHOSPHATE DEHYDROGENASE* (*GAPDH*) of *A.*
266 *thaliana*. Data analysis followed the ΔCT method, based on the subtraction of the CT value of
267 the constitutive gene in relation to the target gene. All experiments were conducted with three
268 biological replicates per condition.

269 ***2.6. DNA extraction and Real time quantitative PCR absolute bacterial quantification***

270 Total DNA extraction was performed using CTAB 2% protocol (Doyle and Doyle,
271 1987). DNA concentration was determined with a NanoDrop™ 2000c spectrophotometer, and
272 its integrity was assessed by electrophoresis in a 1% agarose gel stained with ethidium bromide.
273 Total DNA was treated with 0,01g/mL RNase A and incubated at 37 ºC for 1 h. To determine
274 the bacterial cell number cells (cells g^{-1} plant tissue), the average Ct value from two technical
275 replicates for each DNA sample was used to quantify *G. diazotrophicus* PAL5, *H. seropedicae*
276 HRC54, *A. brasiliense* Ab-V6. Genus-specific standard curve equations, previously
277 established in the laboratory, were applied for quantification. The number of cells were inferred
278 from the amplicon copy number, assuming the target sequence is single copy per genome.
279 Target-specific primer pairs are listed in Table S1. For each treatment, cells per gram of tissue
280 were calculated from the DNA samples using the following equation: Absolute number of cells
281 = A × B (ng μL^{-1}) × C (µL) / D (ng) × E (g). Where, A = number of fragment copies, obtained
282 from the strain-specific standard curve; B = Concentration of extracted genomic DNA; C =
283 volume of DNA extracted; D = amount of DNA used in the qPCR reaction; E = initial plant
284 tissue mass used for DNA extraction.

285 ***2.7. Metagenomic Barcode Analysis***

286 Plants used in the metagenomic barcode analysis experiment were collected at 20 DAG.
287 For each genotype Col-0 wild type and *aip10-1* plants, one sample pool consisting of three
288 plants was collected. Metagenomic barcode analysis experiment was performed exclusively
289 from the root tissue of each genotype. Soil samples were obtained as a sample pool composed
290 of material from the three pots corresponding to the plants whose roots were collected.

291 Total DNA was extracted separately from root and rhizosphere soil samples of
292 *Arabidopsis thaliana* Col-0 and the mutant *aip10-1* using a commercial soil DNA kit. The V3–
293 V4 regions of the bacterial 16S rRNA gene were amplified with universal primers containing
294 Illumina adapters, and amplicon libraries were prepared following standard protocols.
295 Sequencing was performed on an Illumina MiSeq platform (PE 500 bp). Taxonomic
296 assignment was performed against the SILVA 138 database, with removal of non-bacterial
297 sequences. Relative abundance of bacterial taxa was calculated separately for root and soil
298 samples, and results were visualized using GraphPad Prism 10.5.0 for bar plots and
299 comparisons between genotypes. Heatmaps of selected PGPB, diazotrophs, and pathogens
300 were generated in R (pheatmap package), based on log-transformed relative abundances and
301 hierarchical clustering.

302 ***2.8. Confocal microscope and microscopic analysis***

303 Roots of *A. thaliana* ecotype Col-0 wild type and *aip10-1* inoculated with *G. diazotrophicus*
304 Pal5-RFP and *H. seropedicae* RAM10-GFP were analyzed 7 days post inoculation (DAI).
305 Imaging was conducted using a Leica TCS SPE confocal microscope. Plant samples were
306 mounted on microscope slides with a drop of water and covered with a coverslip for
307 observation under a light microscope. For RFP observation (from *G. diazotrophicus* Pal5-
308 RFP), samples were excited at 568 nm and emission was collected at 640 nm. For *H.*
309 *seropedicae* RAM10-GFP (BR 11335), samples were excited at 475 nm and emission was
310 collected at 509 nm. Differential interference contrast (DIC) images were also captured
311 simultaneously using bright field. Image acquisition and processing were performed using
312 Leica LAS AF software.

313

314 **3. Results**

315

316 ***AIP10 expression profile in response to plant growth-promoting bacteria***

317 To first investigate the relationship between PGPB association, plant genotype, and
318 *AIP10* expression, the transcriptional profile of the sugarcane (*Saccharum* spp.) *AIP10*
319 homologue AIP10 homologue was analyzed using previously published RNA-seq datasets
320 from two genotypes well characterized by their contrasting efficiencies in association with
321 beneficial bacteria and in biological nitrogen fixation (BNF) capacity: SP70-1143 (high BNF)
322 and Chunee (low BNF) (Urquiaga and Boddey, 1992; Carvalho *et al.*, 2022). Transcript levels
323 were analyzed in root and shoot tissues from plants grown under natural bacterial colonization
324 and bacteria-free hydroponic conditions. Fold change values (SP70-1143/Chunee) were
325 calculated based on RPKM values to compare the genotype with higher association efficiency
326 with nitrogen-fixing bacteria to the less efficient genotype.

327 Under natural colonization conditions, the *AIP10* homolog exhibited lower expression
328 levels in both roots and shoots of the high-BNF genotype SP70-1143 relative to Chunee (Fig.
329 1A). In contrast, under bacteria-free conditions (BF), *AIP10* expression was upregulated in
330 both tissues of SP70-1143. These results indicate that *AIP10* expression is reduced in the
331 genotype exhibiting higher BNF capacity when associated with beneficial bacteria, supporting
332 its role as a negative regulator of plant growth, and suggesting its modulation may participate
333 in growth promotion in response to beneficial plant-bacteria interaction.

334 A comparative protein domain analysis revealed that AIP10 proteins from *A. thaliana*
335 and sugarcane share a conserved domain architecture, including predicted nuclear localization

336 signals (NLS) and coiled-coil domains (Fig. 1B). This high level of structural conservation
337 suggests a conserved regulatory function of AIP10 across monocot and dicot species. In
338 agreement with these findings, the data revealed a similar *AIP10* expression profile in both
339 plant species, suggesting that these proteins may share similar biological functions.
340 Comparative protein domain analysis of two AIP10 orthologous isoforms in *A. thaliana*
341 (AT1G80940.1 and AT1G80940.3) and one putative isoform in *S. spontaneum*
342 (Sspoon.04G0001710-3D) further confirmed the conservation of nuclear localization and
343 coiled-coil domains, while revealing the presence of an additional ribosomal L32e domain in
344 the sugarcane protein.

345 Next, we investigated the modulation of *AIP10* expression profile by inoculation with
346 beneficial PGPB in wild-type *A. thaliana* Col-0 plants. Plant material was collected at seven
347 days post-inoculation with the diazotrophic PGPB *H. seropedicae* or *G. diazotrophicus,* to
348 assess the *AIP10* transcriptional response during the early stages of plant–microbe interaction
349 (Fig. 1C). The results showed a significant repression of *AIP10* expression in response to both
350 bacterial strains compared to mock-treated controls, with a stronger down-regulation observed
351 upon inoculation with *H. seropedicae* (Fig. 1C). These data suggest that *AIP10* expression is
352 reduced during early stages of plant-PGPB interactions. Together, the results indicate that
353 AIP10 displays a conserved domain architecture across species, while its expression is
354 differentially modulated by bacterial colonization in sugarcane genotypes contrasting for BNF
355 efficiency and in *A. thaliana*.

356 To explore molecular pathways involved in plant–microorganism interactions that are
357 potentially modulated by *AIP10* repression, we analyzed enriched functional categories by
358 reanalyzing previously generated RNA-seq data in the root transcriptomes of *A. thaliana* Col-
359 0 and *AIP10* silenced plants (*aip10-1*) at 11 DAG (Montessoro *et al*., 2025) across metabolic
360 pathways related to Cell wall formation, Response to stimuli, Immune response to bacteria,
361 Responses to hormones, Responses to lipids, Carbohydrates and General metabolic Processes
362 (Fig. S1).

363 Consistent with the enrichment of cell wall–related categories identified in the
364 functional analysis, genes directly involved in cell wall reinforcement and stress-associated
365 remodeling were downregulated (Fig. S1A), including *EXT15* (*Extensin 15*, AT1G23720) and
366 *LRX3* (*Leucine-rich repeat extensin 3*, AT4G13340). The repression of extensins and LRX
367 proteins, which are critical for cell wall assembly, integrity, and mechanical strength, suggests
368 increased cell wall plasticity, that may facilitate bacterial association and root tissue
369 colonization (Kandel *et al.*, 2017). In contrast, a distinct group of proteins associated with cell

370 wall expansion and extracellular matrix organization was significantly induced at 11 DAG,
371 including *GASA1* (Gibberellic Acid Stimulated Arabidopsis 1, AT1G75750) and *LCR69* (Low-
372 molecular-weight Cysteine-rich protein 69, AT2G02100), suggesting enhanced wall loosening
373 and elongation processes. In line with this pattern of cell wall modification, genes encoding
374 enzymes involved in polysaccharide modification and pectin remodeling were also
375 upregulated, including *PME46* (Pectin Methylesterase 46, AT5G04960), *XHT* (Xyloglucan
376 endotransglucosylase/hydrolase, AT4G25820), and *ATTIP2* (Tonoplast Intrinsic Protein 2,
377 AT3G16240), suggesting an active restructuring of the polysaccharide network that controls
378 wall extensibility and porosity in *aip10-1* plants, which may enhance apoplastic permeability
379 and promote cell-to-cell communication (Dora *et al.*, 2022)

380 Other genes positively related to processes involved in plant growth promotion by
381 PGPB were upregulated in *aip10-1* plants. In the hormone-responsive category, the auxin-
382 responsive genes *SAUR69* (Small Auxin Upregulated RNA 69) and *SAUR72* (Small Auxin
383 Upregulated RNA 72) were strongly upregulated, suggesting a role in promotion of plant
384 growth. Class I ROOT HAIR DEFECTIVE SIX-LIKE 4 (RSL4) basic helix–loop–helix
385 (bHLH85) transcription factor, that positively regulates root hair development, was
386 upregulated in *aip10-1* roots.

387 Transcriptome analyses of *aip10-1* plants revealed both repression and induction of
388 genes involved in defense or response pathways to bacterial interaction, required for beneficial
389 associations with PGPB (Stringlis *et al.*, 2018). Among the most downregulated genes were
390 *CYP71A12* and *CYP71A13* (Cytochrome P450 71A12 and– Cytochrome P450 71A13), which
391 are key enzymes involved in camalexin and tryptophan-derived secondary metabolite
392 biosynthesis. Their repression suggests a reduction in chemical defense pathways. In contrast,
393 a distinct subset of bacterium-responsive genes was strongly induced, reflecting activation of
394 regulatory pathways associated with plant–microbe communication and systemic signaling. A
395 subset of stimulus-related genes, including *PDF2.2* (*Plant Defensin 2.2*), *ATL15* (*RING-type*
396 *E3 ubiquitin ligase 15*), AT1G22770, and AT1G15010, was induced, suggesting the activation
397 of regulatory and antimicrobial components that may contribute to controlling the number of
398 bacteria that could associate with and colonize the root tissue. The most strongly induced gene
399 was *ILA* (ILITHYIA), which displayed a marked transcriptional activation, suggesting a central
400 role in coordinating developmental and immune signaling (Faus *et al.*, 2018).

401 The regulation of metabolic, lipid, and carbohydrate-responsive genes in *aip10-1*
402 revealed a coordinated transcriptional reprogramming affecting primary metabolism and stress-
403 associated pathways. Repression of *PAD3* (Phytoalexin Deficient 3) and *CBP60G*

404 (Calmodulin-Binding Protein 60G) supports an attenuation of defense-associated metabolic
405 pathways, indicating a general downregulation of stress- and defense-related metabolic
406 programs. Within this metabolic shift, genes involved in carbohydrate-associated processes
407 also displayed a regulatory adjustment. In the carbohydrate response pathway, repression of
408 *GLS1* (Glucan Synthase-Like 1) together with induction of *ATL15* (RING-Type E3 Ubiquitin
409 Ligase 15) suggests a reprogramming of carbon-related regulation, suggesting an adjustment
410 of carbohydrate metabolism rather than a simple reduction in carbon availability.

411 Together, the transcriptional changes observed in *AIP10*-silenced plants reveal
412 modulation of core metabolic processes combined with regulatory control of defense and
413 growth-related pathways, consistent with a transcriptional reprogramming associated with
414 plant responses to beneficial endophytic or associative PGPB and aligned with the reduced
415 *AIP10* expression observed under natural bacterial colonization in sugarcane.

416

417 ***Root-associated microbiota composition in A. thaliana wild-type and aip10-1 plants***

418 Given that transcriptional reprogramming in *aip10-1* plants affects multiple pathways
419 related to plant–microbe interactions, we next examined whether AIP10 silencing alters the
420 composition of the root-associated microbiota in *A. thaliana*. A metagenomic barcode analysis
421 of the root-associated bacterial communities and the rhizosphere soil of non-inoculated Col-0
422 and *aip10-1* plants was performed.

423 The Venn diagram revealed a complex distribution of shared and unique taxa among
424 the four sample types, comprising soil and roots from both genotypes. Col-0 and *aip10-1* roots
425 each harbored a high number of genotype-specific bacterial species (237 and 203, respectively)
426 (Fig. 2A), indicating distinct recruitment patterns. Despite these differences, a substantial core
427 microbiome of 975 bacterial species was shared across all samples, highlighting a conserved
428 microbial baseline between soil and plant genotypes. Additionally, soil samples associated with
429 Col-0 and *aip10-1* each contained unique taxa (173 and 220 species, respectively (Fig. 2A),
430 reflecting environmental and genotype-driven filtering effects. Together, these findings
431 demonstrate that *AIP10* silencing reshapes root-associated bacterial communities while
432 maintaining a large portion of shared microbial taxa.

433 For a more focused assessment of functionally relevant components of the native
434 microbiome potentially associated with growth promotion and innate immune responses in the
435 host plant, the abundance of selected bacterial categories was analyzed by z-score values (Table
436 S1), including potential diazotrophic bacteria, PGPB, and plant pathogenic bacteria.

437 Comparative profiling of bacterial communities associated with the plant root
438 compartment revealed pronounced differences between Col-0 and *aip10-1* genotypes (Fig. 2B-
439 C). At the species level, roots of *aip10-1* plants exhibited increased relative abundance of
440 several potential diazotrophic bacteria, including, *Azospirillum brasilense* (z-score 1,4),
441 *Azospirillum halopraferens* (z-score 1,5), *Bradyrhizobium elkanii* (z-score 1,4) and
442 *Bradyrhizobium guangxiense* (z-score 0,9). In addition, plant PGPB species were enriched in
443 *aip10-1* roots in comparison with Col-0 roots, as *Paenibacillus medicaginis* (z-score 0,9) (Fig.
444 2C).
445 In contrast, roots of Col-0 plants displayed higher relative abundance of several
446 pathogenic species, compared to *aip10-1* roots (Fig. 2D). Taxa such as *Xanthomonas*
447 *arboricola* (z-score 1,5), *Xanthomonas axonopodis* (z-score 0,5), *Pantoea brenneri* (z-score
448 1,5), and *Erwinia soli* (z-score 0,4) were comparatively more abundant in Col-0 and were not
449 detected in *aip10-1*. These data suggest that *aip10*-1 plants tend to preferentially recruit and
450 associate with specific beneficial PGPB species in the root compartment while being depleted
451 in potentially pathogenic taxa.
452 A similar pattern was observed in soil-associated bacterial communities (Fig. 2B-C).
453 Soils cultivated with *aip10-1* plants were characterized by increased relative abundance of
454 several potential diazotrophic species, including *Mesorhizobium composti* (z-score 31,2),
455 *Mesorhizobium gobiense* (z-score 52,7), *Mesorhizobium hankyongi* (z-score 1,0),
456 *Mesorhizobium silamurunense* (z-score 3,7) *Azospirillum formosense* (z-score 1,5),
457 *Burkholderia alpina* (z-score 6,3), *Burkholderia ultramafica* (z-score 0,7), when compared
458 with soils from Col-0 plants. Likewise, PGPB species such as *Paraburkholderia diazotrophica*
459 (z-score 1,1), *Paraburkholderia megapolitana* (z-score 1,2), *Paraburkholderia metrosideri* (z-
460 score 0,9) and *Bradyrhizobium canariense* (z-score 0,9) were more abundant in soils associated
461 with *aip10-1*.
462 On the other hand, soils from Col-0 plants harbored higher relative abundances of
463 potential pathogenic species (Fig. 2D), including *Xanthomonas campestris* (z-score 1,5),
464 *Xanthomonas translucens* (z-score 1,5), *Erwinia billingiae* (z-score 1,5), and *Agrobacterium*
465 *larrymoorei* (z-score 1,5).
466 Together, these results suggest that the loss of AIP10 function reshapes the root-
467 associated bacteria in roots and rhizospheric soil, increasing the prevalence of beneficial
468 bacteria while reducing potential pathogens.
469
470 ***Efficiency of PGPB based-bioinoculant colonization in aip10-1 plants***

471 As *AIP10* silenced mutants showed an increased abundance of beneficial bacteria in
472 their root microbiome, we next investigated whether *aip10-1* mutants exhibit enhanced
473 colonization in response to inoculation with diazotrophic PGPB-based bioinoculants,
474 compared to wild-type Col-0 plants, by quantifying and assessing the dynamics of bacterial
475 root colonization.

476 Inoculation experiments were performed with two nitrogen-fixing bacterial strains, *G.*
477 *diazotrophicus* PAL5 and *H. seropedicae* HRC54. Representative images of *aip10-1* plants 20
478 DAG, inoculated with either strain, are shown in Fig. 3A. Under in vitro growth conditions,
479 root architectural parameters were evaluated revealing that inoculated *aip10-1* plants displayed
480 a significant increase in primary root length compared with mock-treated plants and inoculated
481 Col-0 controls (Fig. 3B). In addition, the number of lateral roots was significantly higher in
482 inoculated *aip10-1* plants, particularly in response to PAL5 (Fig. 3C).

483 To determine whether these early root architectural changes translate into later
484 developmental outcomes, shoot-related traits were assessed at later developmental stages. On
485 21 DAG *aip10-1* plants inoculated with both bacterial strains accumulated significantly higher
486 shoot biomass (Fig. 3D) and developed larger rosette areas compared with Col-0 plants and
487 mock-treated controls (Fig. 3E).

488 Quantification of bacterial colonization based on absolute values of single-copy
489 bacterial gene using genus-specific primers showed that *aip10-1* roots of inoculated plants were
490 better colonized by both bioinoculants, compared to wild-type Col-0 roots (Fig. 3F and G). To
491 evaluate if the higher colonization by *G. diazotrophicus* or *H. seropedicae* was correlated with
492 actively metabolic bacteria, *nifH* mRNA expression was analyzed. The *nifH* is present in most
493 diazotrophic microorganisms and encodes a key component of nitrogenase, making it an ideal
494 marker for assessing the stimulation of N_2-fixation metabolism in bacterial communities
495 (Nichio *et al.*, 2025). As shown in Fig. 3H and I, PGPB-inoculated *aip10-1* plants showed
496 significantly higher relative expression of *nifH* than inoculated wild-type plants during
497 association with both HRC54 or PAL5, respectively.

498 To investigate whether *aip10-1* mutants affect the niche of bacterial colonization in root
499 tissues, RFP- and GFP-labeled G. *diazotrophicus* and *H. seropedicae* bacteria, respectively,
500 were used as bioinoculants and monitored by confocal microscopy. The data showed
501 differences in Col-0 and *aip10-1* roots in relation to the pattern of bacterial colonization. In
502 mock Col-0 roots, both RFP- and GFP-labeled bacteria showed minimal and discontinuous
503 fluorescence, indicating low colonization levels. In contrast, inoculated *aip10-1* roots displayed
504 strong and spatially extended fluorescent signals, with well-defined aggregates and continuous

505 bands along the root surface (Fig. 3J). A detailed analysis of distinct root regions further
506 demonstrated that these differences were spatially structured. In the meristematic zone, both
507 genotypes exhibited low colonization (Fig. S2). However, beginning in the root hair zone,
508 *aip10-1* showed a marked increase in bacterial attachment, with continuous fluorescent bands
509 extending along the root axis. This pattern became more evident in the elongation zone, where
510 large portions of the cortex and epidermis were covered by bacteria, in sharp contrast to the
511 fragmented and sparse pattern observed in Col-0 (Fig. S2). The highest colonization levels
512 were observed at lateral root emergence sites, where inoculated aip*10-1* roots displayed
513 extensive and well-defined bacterial aggregates, whereas Col-0 presented only small, scattered
514 foci. Together, these spatial colonization patterns indicate that loss of *AIP10* enhances root
515 colonization, particularly in regions of active growth and lateral root formation, resulting in
516 greater density, continuity, and stability of bacterial association.
517 Together, these results indicate that AIP10 silencing is associated with enhanced
518 bacterial colonization and activity in roots, accompanied by pronounced changes in root
519 architecture and shoot growth following inoculation.
520
521 ***Mechanisms of plant growth in PGPB based-inoculated aip10-1 plants***
522 As *AIP10* silenced mutants showed increased root colonization by beneficial bacteria
523 and enhanced plant growth promotion, compared to wild-type Col-0 plants, we investigated
524 the molecular mechanisms that may contribute to the improved responsiveness of *aip10-1*
525 plants to PGPB-based bioinoculants.
526 First, we investigated the modulation of cell division controls in inoculated *aip10-1* and
527 Col-0 plants. AIP10 has previously been described as a negative modulator of cell division,
528 through its interaction with ABAP1 and regulation of ABAP1 pathway target gene expression
529 (Montessoro *et al.*, 2025). Also, *ABAP1* expression is negatively regulated in *aip10-1* mutants.
530 Therefore, the expression levels of *ABAP1* and *CDT1a*, a target gene negatively regulated by
531 ABAP1 and a positive marker of DNA replication, were evaluated by RT-qPCR (Fig. 4). In
532 *aip10-1* plants, *ABAP1* expression was more strongly repressed in response to inoculation with
533 PAL5 and HRC54 compared to mock-treated mutants, whereas inoculated Col-0 plants
534 consistently showed higher *ABAP1* expression than *aip10-1* mutants (Fig. 4A). Accordingly,
535 *CDT1a* expression was induced in *aip10-1* plants in response to both beneficial inoculations,
536 with PAL5 triggering significantly higher induction than in mock-treated plants (Fig. 4B).
537 Expression of the cell division marker *CYCB1;1* was strongly induced in inoculated *aip10-1*
538 mutant plants compared to mock-treated controls, suggesting that beneficial bacterial

539 colonization stimulate higher cell division rates in *aip10-1* plants (Fig. 4C). Overall, increased
540 colonization by PGPB-based bioinoculants in *aip10-1* mutant plants enhanced the
541 transcriptional regulation of ABAP1 and genes associated with this pathway, consistent with
542 the growth promotion observed upon inoculation.

543 Next, based on previously reported RNAseq data from non-inoculated Col-0 and *aip10-*
544 *1* plants (Montessoro et al., 2025), three genes related to cell wall organization, defense against
545 bacteria, or root hair development were selected for expression analysis in roots under
546 beneficial inoculation (Fig. S1). Leucine-rich repeat extensins (LRXs) are extracellular
547 proteins composed of an N-terminal leucine-rich repeat (LRR) domain and a C-terminal
548 extensin domain (Draeger *et al.*, 2015) Among the 11 *LRX* genes in *A. thaliana*, *LRX3, LRX4*
549 and *LRX5* perform redundant functions associated with the regulation of plant growth and cell
550 wall formation, predominantly expressed in leaves and stems (Draeger *et al.*, 2015). *LRX3* and
551 *LRX4* were downregulated in *aip10-1* compared to Col-0 according to transcriptomic data.
552 Consistently, validation analysis revealed reduced *LRX4* expression in *aip10-1* mock-treated
553 plants, with no change upon bacterial inoculation when compared to wild-type plants (Fig. 4D).
554 Furthermore, we evaluated the expression of *ILITYHIA* (*ILA*), which was found to be
555 upregulated in *aip10-1* in the transcriptome analysis. *ILA* is required for plant immunity, being
556 directly associated with basal defense in *A. thaliana* against the pathogenic bacteria
557 *Pseudomonas syringae* (Monaghan and Li, 2010). Here, *ILA* expression was higher in both
558 *aip10-1* mock and inoculated plants, compared to Col-0, supporting the transcriptomic data and
559 suggesting that some plant defense responses may be basally active in *aip10-1* mutants (Fig.
560 4E). Enhanced root hair growth is a commonly reported response to inoculation with PGPB
561 (Zhao et al., 2025). Transcriptomic data revealed a positive regulation of *RSL4* (bHLH85,
562 ROOT HAIR DEFECTIVE 6-LIKE 4) in *aip10-1* roots, which was corroborated by RT–qPCR
563 analyses showing higher expression levels in mock-treated *aip10-1* plants compared to Col-0,
564 with expression remaining elevated in the presence of both bacterial strains (Fig. 4F). Our
565 analyses showed that gene expression profiles were largely similar between non-inoculated and
566 inoculated *aip10-1* plants, including genes related to cell wall dynamics and bacterial
567 responses. This lack of transcriptional modulation upon inoculation suggests that *aip10-1*
568 mutants may already exhibit a basal transcriptional state associated with beneficial plant–
569 microorganism interactions, potentially reflecting their enhanced capacity to naturally
570 associate with PGPB, as supported by the root-associated microbiome composition observed
571 under non-inoculated conditions.

572 **Response of *aip10-1* plants to association with diazotrophic PGPB-based bioinoculants**
573 **under high and low fertilization conditions**

574 Given the improved efficiency of the association between *aip10-1* plants and PGPB-
575 based bioinoculants, as well as increased *nifH e*xpression indicating higher nitrogenase activity
576 in *aip10-1* roots, we investigated whether inoculation of aip*10-1* mutant plants could reduce
577 their dependence on mineral fertilization. To address this question, inoculation responses of
578 *aip10-1* and wild-type Col-0 plants were analyzed under conditions of low and high nutrient
579 availability.

580 Initially, an *in vitro* inoculation system followed by greenhouse cultivation was
581 established to study the interaction of *aip10-1* mutant plants with *H. seropedicae* HRC54 or
582 *G. diazotrophicus* Pal5, or a commercial bioinoculant (Biofree) containing the strains *A.*
583 *brasilense* Ab-V6 and *P. fluorescens* CCTB03, with the aim of characterizing phenotypic and
584 molecular responses under low (0.06 g/L NPK; 20:20:20, corresponding to 12 mg/L N, 5.2
585 mg/L P and 10 mg/L K) and high (0.12 g/L NPK; 20:20:20, corresponding to 24 mg/L N, 10.4
586 mg/L P and 20 mg/L K) nutrient availability. Four treatment groups were established for both
587 Col-0 and *aip10-1* plants: i) mock-treated plants grown under low fertilization, ii) mock-treated
588 plants grown under high fertilization, iii) plants inoculated with the HRC54 or PAL5 or Biofree
589 grown under low fertilization, iv) plants inoculated with the HRC54 or PAL5 or Biofree grown
590 under high fertilization (Fig. S3). First, root colonization with the PGPB-based bioinoculants
591 (HRC54 or Pal5 or Biofree) was validated in plants at 7 DAI, before starting differential
592 fertilization treatments, through absolute quantification of a single-copy bacterial gene using
593 genus-specific primers by qPCR (Fig. 3F-G and Fig. S4). Bacterial counts showed that *aip10-*
594 *1* plants have a higher number of bacterial cells per gram of plant tissue compared to Col-0,
595 suggesting a better interaction of mutant plants with the bioinoculants.

596 The effects of fertilization with high or low doses of nutrients were analyzed in the
597 shoots and roots at 35 DAG, which corresponds to 31 DAI (Fig. 5A and B). Our results showed
598 that *aip10-1* plants were more responsive to bioinoculants under low nutrient availability,
599 exhibiting enhanced growth, like the phenotype observed in mock-treated mutant plants grown
600 in environments with high fertilizer availability. In shoot, this beneficial effect was observed
601 through analyses of rosette area and dry biomass, where *aip10-1* plants presented 22%
602 (HRC54) (Fig. 5C) and 26% (Pal5) (Fig. 5F) larger area, as well as 33% (HRC54) (Fig. 5D)
603 and 35% (Pal5) (Fig. 5G) greater dry weight when inoculated under low nitrogen availability
604 compared to Col-0 plants under the same conditions. Furthermore, rosette area and dry biomass

605 increased by 30% (Fig. 5C and F) and 42% (Fig. 5D and G), respectively, in mock-treated
606 *aip10-1* mutant plants under conditions of high fertilizer availability. Chlorophyll content
607 analyses demonstrated this same pattern, with an increase in response to both inoculations in
608 *aip10-1* plants compared to wild-type plants under low fertilization conditions (Fig. 5E and H),
609 consistent with the increase observed in mock mutant plants grown under high fertilization,
610 corroborating previous results. Parallel experiments were conducted using a commercial
611 bioinoculant, Biofree, containing the strains *A. brasilense* Ab-V6 and *P. fluorescens* CCTB03.
612 Under low nutrient availability, *aip10-1* plants inoculated with Biofree exhibited a marked
613 increase in rosette expansion and biomass accumulation compared with mock-treated mutants
614 (Fig. S4). Again, this growth promotion was comparable to that observed in mock-treated
615 *aip10-1* plants grown under high nutrient conditions (Fig. S4).
616 Regarding root phenotypic analyses, plants with reduced *AIP10* levels exhibited more
617 developed root systems in response to inoculation with the HRC54 and Pal5 strains upon low
618 fertilization (Fig. 6). Under these conditions, *aip10-1* plants inoculated with HRC54 and Pal5
619 exhibited 20–51% longer roots (Fig. 6B and E) and 24–42% larger surface area (Fig. 6C and
620 F) compared to Col-0, respectively. At the same time, under high fertilization, non-inoculated
621 *aip10-1* plants still exhibited average increases of 40% in root length and 50% in surface area
622 relative to wild-type plants (Fig. 6B-C and 6E-F). The increased root growth of *AIP10* mutants
623 resulted in a significant increase in dry matter. In response to beneficial inoculation, the gain
624 in root dry matter ranged from 40% (Fig. 6A) to 70% (Fig. 6D) in mutant plants relative to
625 wild-type plants under low fertilization, equivalent to the increase found in *aip10-1* mock-
626 treated plants grown under high fertilization. Also, under low-nutrient conditions, Biofree
627 inoculation markedly enhanced root biomass, elongation, and surface area in mutant plants,
628 while producing no increases in Col-0 (Fig. S5).
629 The use of bioinoculants also promoted positive changes at the plant reproductive stage
630 (Fig. 7A). Consistent with the results for the vegetative phase, low fertilization positively
631 influenced the height of the main inflorescence axis in inoculated mutant plants, with an
632 average increase of approximately in response to both inoculations compared to Col-0 (Fig. 7B
633 and E). In addition, this combination of stimuli generated inflorescences with 23–29% more
634 siliques on the main axis of inoculated *aip10-1* plants compared to all other groups grown under
635 low fertilization (Fig. 7C and F). Similarly, *AIP10* mutants produced a higher total seeds weight
636 even under low fertilization conditions, due to the inoculation of HRC54 (Fig. 7D) and Pal5
637 (Fig. 7G). Additionally, the commercial microbial consortium more strongly enhanced silique
638 number and total seed yield in *aip10-1* than in Col-0, particularly under nutrient limitation (Fig.

639 S6). Overall, *AIP10* mutants responded better to the bioinoculants containing diazotrophic
640 bacteria, resulting in greater dry biomass accumulation in both shoots and roots compared to
641 Col-0 plants. Moreover, these benefits were primarily evident under low-fertilization
642 conditions. Taken together, the results suggest that the use of bioinoculants can largely replace
643 the use of mineral fertilizers in *aip10-1* mutant plants.
644
645 **Nitrogen metabolism in *aip10-1* plants associated with diazotrophic PGPB under high**
646 **and low fertilization conditions**
647 Our data showed that PGPB inoculation in *aip10-1* increased bacterial *nifH* expression
648 and had additive effects on plant biomass and chlorophyl levels, partially compensating for the
649 need for chemical fertilizers. We therefore investigated N assimilation in *aip10-1* plants by
650 analyzing the expression of representatives in two selected key gene families known to respond
651 to changes in nitrogen availability and PGPB inoculation (Rosman *et al.*, 2024). The N
652 assimilation genes analyzed were: i) the two Nitrate Reductases (NR) *NIA1* and *NIA2* that
653 are modulated by nitrate availability (Wilkinson and Crawford, 1993); ii) and the two
654 Glutamine Synthetase cytosolic genes (GS1), *GLN1;1* and *GLN1;3,* that are high-affinity and
655 low-affinity-related isoforms, respectively (Ishiyama *et al.*, 2004). Analyzes were performed
656 by RT-qPCR of root samples collected at 20 DAG from wild-type and *aip10-1* plants in mock-
657 treated or inoculated and grown in a greenhouse under the two fertilization conditions.
658 We first evaluated the N metabolism data in mock-treated plants, as the native
659 microbiome in non-inoculated *aip10-1* root compartment was enriched with PGPB and
660 diazotrophic bacteria. Consistent with the microbiome data, Fig. 8A showed higher levels of
661 *nifH* expression in *aip10-1* mock-treated plants cultivated under low nutrients. *NIA1* and *NIA2*
662 showed similar expression patterns (Fig. 8B and C), being induced under high nutrients
663 availability in non-inoculated *aip10-1* plants compared to wild-type ones and showing no
664 modulation in response to low nutrients condition (Fig. 8B and C). Under both nutritional
665 conditions, mock-treated *aip10-1* plants showed a tendency towards higher levels of *GLN1;1*
666 expression compared to Col-0 (Fig. 8D); and *GLN1;3* was up-regulated in mock-treated *aip10-*
667 *1* mutants relative to Col-0 under high nutrient availability (Fig. 8D). Taken together, these
668 data suggest that *AIP10* silencing can activate ammonium and nitrate assimilation pathways,
669 particularly in roots exposed to high nutrient availability. *aip10-1* potentially supports a more
670 efficient nitrogen assimilation compared to wild-type plants, consistent with the enhanced
671 biomass accumulation previously reported for *aip10-1* under high nutrient conditions.
672 Furthermore, we evaluated how nutrient availability affects *nifH* expression in natural

673 microbiomes associated with wild-type and *aip10-1* plants. The results revealed that low
674 nutrient availability boosted *nifH* expression in *aip10-1* mock compared with high-nutrient
675 conditions or non-inoculated controls (Fig. 8F).

676 Given that in this study we observed increased growth promotion in *aip10-1* plants
677 when associated with N_2-fixing bioinoculants under low nutrient availability, we investigated
678 whether inoculation with diazotrophic bacteria affected regulation of nitrogen assimilation
679 enzymes. Initially, we evaluated the effect of nutrient availability on *nifH* expression in
680 diazotrophic bacteria associated with Col-0 and *aip10-1* plants. Low nutrient availability
681 increased *nifH* expression in *aip10-1* plants inoculated with HRC54 and Pal5 relative to high-
682 nutrient conditions or non-inoculated controls (Fig. 9A and B). Under low nitrogen conditions,
683 *GLN1;1* expression displayed similar patterns in *AIP10*-silenced plants in response to both
684 inoculations, with a trend toward higher expression but no difference relative to mock controls
685 or to mutant plants grown under high nutrient availability (Fig. 9C and D). These data suggest
686 that, despite *nifH* activation, growth promotion by diazotrophic bacteria may not be restricted
687 to N_2 fixation. By contrast, under low nitrogen fertilization, *H. seropedicae* inoculation
688 significantly increased *NIA1* expression in *aip10-1* plants relative to other inoculated groups
689 grown under high or low nitrogen, whereas *G. diazotrophicus* inoculation had no effect on
690 *NIA1* expression (Fig. 9E and F). Rather than reflecting a direct increase in nitrogen
691 availability, the induction of *NIA1* in *aip10-1* plants following bacterial inoculation may be
692 associated with improved nitrogen use efficiency, mediated by multiple plant growth-
693 promoting mechanisms, including hormonal modulation and potential restructuring of the root-
694 associated microbiome.
695
696 **4. Discussion**
697
698 Achieving high agricultural productivity while minimizing environmental harm requires
699 the adoption of novel and sustainable approaches that limit dependence on mineral fertilizers.
700 PGPB-based bioinoculants represent a promising strategy to enhance crop performance while
701 reducing reliance on mineral fertilizers. However, their effectiveness is highly variable and
702 largely depends on plant genetic factors that regulate microbial recruitment and colonization.
703 Although plants actively shape their root-associated microbiota, the molecular mechanisms that
704 enable the accommodation of beneficial PGPB without triggering defense responses remain
705 poorly understood (Vandenkoornhuyse *et al.*, 2015; Zhang *et al.*, 2023). Elucidating these
706 plant-controlled processes is critical for improving the consistency of PGPB-plant interactions.

707 Our research group has systematically investigated the molecular basis of plant-PGPB
708 communication, identifying key signaling, transcriptional, and metabolic pathways that are
709 modulated during these interactions ultimately influencing plant physiological and
710 developmental responses (Carvalho *et al.*, 2011, 2016, 2022; Thiebaut *et al.*, 2017; Hardoim *et*
711 *al.*, 2020; Ballesteros *et al.*, 2021; Rosman *et al.*, 2024). Here we investigated whether a plant
712 growth regulatory network integrating cell-cycle and metabolic regulation contributes to
713 beneficial interactions with PGPB in the endogenous root microbiome or in response do PGPB-
714 bioinoculants. Within this network, AIP10 acts as a negative regulator, and its silencing results
715 in healthier plants with increased biomass and yield, along with enhanced metabolite
716 accumulation (Montessoro *et al.*, 2025). We have demonstrated that silencing of *AIP10*
717 promotes changes in root architecture, characterized by increased lateral root formation, and
718 triggers the regulation of multiple metabolic pathways associated with development, cell wall
719 remodeling, immune responses, and metabolite biosynthesis, suggesting a physiological
720 reprogramming that may favor plant interactions with PGPB. These findings converged on a
721 central question of this work: to what extent do the molecular frameworks governing plant-
722 bacteria communication and those controlling cell division and metabolism are integrated?
723
724 ***AIP10* silencing favors beneficial microbial recruitment**
725 Consistent with evidence that plant genes shape root-associated bacterial communities,
726 we found that loss of *AIP10* function in *A. thaliana* reshaped root-associated bacterial
727 communities while maintaining a substantial core of shared taxa. Notably, *aip10-1* plants
728 preferentially recruited beneficial PGPB, particularly diazotrophic PGPB, in both the root
729 compartment and rhizospheric soil, while being depleted in potentially pathogenic taxa. Based
730 on recent advances in root microbiome research, we can hypothesize about the mechanisms
731 underlying PGPB recruitment in *aip10-1* plants.
732 Increasing evidence suggests that plant performance and environmental adaptation rely
733 on coordinated interactions with the root microbiota. Genes governing development, immune
734 responses, nutrient uptake, and metabolite release were shown to possibly function as
735 determinants of the microbiome assembly (Zhang *et al.*, 2023). AIP10 plays an important role
736 in modulation of plant development, to adapt to the environment, and *aip10-1* plants show
737 improved performance (Montessoro *et al.*, 2025). In rice, NRT1.1B, a nitrate transporter and
738 sensor, was associated with modulation of root microbiota composition, integrated with higher
739 NUE in field-grown plants (Zhang *et al.*, 2019). Consistent with this mechanism, non-
740 inoculated *aip10-1* plants showed higher expression of nitrogen assimilation genes compared

741 to Col-0, along with a root microbiota enriched in PGPR and diazotrophic bacteria that enhance
742 nitrogen availability to the plant.

743 The mechanisms by which *aip10-1* re-shapes its root microbiome toward the
744 enrichment of beneficial PGPB, particularly diazotrophic bacteria, may involve alterations in
745 plant carbon metabolism and allocation. Carbohydrate levels were quantitatively increased in
746 leaves of *aip10-1* plants indicating changes in primary metabolism (Montessoro *et al.*, 2025).
747 Consistently, in the present study, genes associated with carbohydrate metabolic pathways
748 were differentially expressed, suggesting altered carbon availability that could support the
749 recruitment of diazotrophic PGPB, for which carbohydrates represent key nutrient sources
750 (Upadhyay *et al.*, 2022; Hemelda and Noutoshi, 2025). There is evidence that plant metabolites
751 can play a selective role, as root-derived metabolites actively shape the root microbiome, with
752 specific plant genes influencing microbial recruitment, community structure, and function
753 (Vandenkoornhuyse *et al.*, 2015; Zhang *et al.*, 2023). Loss-of-function mutations in genes
754 controlling coumarin biosynthesis or export significantly modify rhizosphere and endosphere
755 communities, promoting the recruitment of growth-promoting or nutrient-mobilizing bacteria
756 through changes in root-derived specialized metabolites (Stringlis *et al.*, 2018; Huang *et al.*,
757 2019; Voges *et al.*, 2019). Secondary metabolites such as phenolics and terpenes have been
758 shown to modulate microbiome composition and enrich beneficial taxa (Stringlis *et al.*, 2018;
759 Harbort *et al.*, 2020). Furthermore, genotype-specific metabolites explain substantial
760 microbiome variation in crops such as rice (Liu *et al.*, 2025).

761 In parallel, silencing of *AIP10* lead to major transcriptional reprogramming, including
762 genes in pathways related to plant-microorganism interaction such as cell wall formation,
763 defense, immune response to bacteria and hormonal responses. In *aip10-1* roots, modulation
764 of cell wall–related genes suggest increased cell wall plasticity. Genes involved in cell wall
765 loosening, such as *XTH* and *PME46*, were induced, whereas genes associated with cell wall
766 reinforcement and stress-related remodeling, including *EXT15* and *LRX3*, were repressed. This
767 shift may facilitate bacterial association and root tissue colonization.

768 The transcriptional profile of *aip10-1* plants resembles signatures reported in genotypes
769 with enhanced capacity to interact with beneficial microorganisms. In sugarcane, genotypes
770 that efficiently associate with endophytic diazotrophic bacteria show extensive reprogramming
771 of cell wall–modifying genes, promoting increased tissue plasticity and microbial
772 accommodation (Ballesteros *et al.*, 2021). Consistent with this, broader evidence indicates that
773 cell wall remodeling is a key feature of plant readiness for symbiotic or associative interactions,
774 as exposure to PGPR commonly induces expansins and XTHs across diverse plant species

775 (Vacheron *et al.*, 2013; Srivastava *et al.*, 2023). The similarity between these microbial-induced
776 responses and the transcriptional profile of *aip10-1* roots, even in the absence of bacterial
777 inoculation, suggests that *AIP10* silencing may promote a pre-accommodative or primed state
778 characterized by increased cell wall flexibility and altered root surface properties.

779 In *aip10-1* plants, genes involved in immune and defense pathways related to bacterial
780 interactions were either repressed or induced. Such transcriptional reprogramming is required
781 for successful beneficial associations with PGPB, as plants must downregulate specific defense
782 responses to permit bacterial colonization while simultaneously activating other defense
783 pathways to prevent bacterial overgrowth (Carvalho *et al.*, 2016). Alterations in innate
784 immunity pathways also lead to distinctive microbial assemblages, as shown in mutants
785 impaired in pattern-recognition receptors, which exhibit shifts in core bacterial taxa and
786 increased abundance of taxa typically associated with beneficial functions (Ma *et al.*, 2021).
787 Upregulation of bacterial response regulators such as ILA in *aip10-1* is consistent with plants
788 genetically primed for beneficial microbial associations showing enhanced sensitivity to
789 microbe-derived signals before colonization (Liu *et al.*, 2017; Gao *et al.*, 2022). Although ILA
790 regulates immunity, its association with salicylic acid (SA) signaling may help offset the costs
791 of accelerated growth by activating defense responses or increasing stress tolerance.
792 Consistently, disruption of salicylic acid (SA) signaling was shown to alter the abundance of
793 specific microbial groups in the Arabidopsis rhizosphere, supporting immune pathways as key
794 determinants of microbiota structure (Lebeis *et al.*, 2015). ERF1 (Ethylene Response Factor 1)
795 was strongly induced in *aip10-1* roots, indicating activation of ethylene-responsive pathways
796 involved in growth regulation and stress signaling. Taking together, the transcriptional
797 reprogramming in *aip10-1* does not reflect a fully activated or suppressed immune system, but
798 rather an intermediate immune state. This state appears to alter how roots perceive and respond
799 to soil microorganisms, creating a more permissive environment for colonization by
800 diazotrophic and PGPB-enriched taxa while limiting the presence of potential pathogens.
801

802 **Enhanced growth promotion in *aip10-1* in response to PGPB inoculation are driven by**
803 **coordinated activation of cell division and nitrogen metabolism**

804 Consistent with a native root microbiota enriched with beneficial bacteria, inoculated
805 *aip10-1* genotype was colonized by higher numbers of PGPB-based bioinoculant during early
806 phases after inoculation. Consequently, *aip10-1* plants exhibited increased root and shoot dry
807 biomass and higher productivity in response to inoculation with *G. diazotrophicus* Pal5 and *H.*

808 *seropedicae* HRC54, compared to inoculated wild-type plants. Previous studies in sugarcane
809 and maize have shown that plant-PGPB associations modulate the expression of gene clusters
810 related to nitrogen metabolism, root development, cell wall modification, defense and immune
811 responses and hormonal responses (Hardoim *et al.*, 2020; Ballesteros *et al.*, 2021; Rosman *et*
812 *al.*, 2024). In the previous topic, the transcriptional modulation of these pathways was
813 discussed as possible mechanisms that support the high abundance of PGPB in non-inoculated
814 *aip10-1* microbiota. In PGPB-inoculated *aip10-1* plants, we have further investigated the
815 mRNA levels of selected genes involved in immune response (*ILA)*, cell wall modification
816 *(LRX4)* and root development (*RSL4*), and compared to the expression profile in no-inoculated
817 plants. Our analyses showed that gene expression profiles were similar between non-inoculated
818 and inoculated *aip10-1* plants, possibly because the beneficial bacteria effects were already
819 present in the non-inoculated mutants. However, the enhanced traits observed in non-
820 inoculated *aip10-1* plants were further amplified upon inoculation, indicating additive effects
821 on plant growth promotion.

822 Beneficial plant-bacteria associations can directly stimulate plant growth and
823 development through several mechanisms including BNF and phytohormone production,
824 primarily improving nutrient use efficiency (Thiebaut *et al.*, 2022). Increased biomass
825 ultimately depends on higher rates of cell division, as plant growth and morphogenesis are
826 governed by the balance between cell division, cell expansion, and cell differentiation
827 (Jorgensen and Tyers, 2004; Jones *et al.*, 2017; Carneiro *et al.*, 2021). Because AIP10 is part
828 of a regulatory network that controls plant growth by modulating cell cycle progression at G1
829 to S phase, a key checkpoint regulated by environmental signals, such as biotic interactions
830 (Masuda *et al.*, 2008; Montessoro *et al.*, 2025), we investigated whether this network
831 contributes to the improved performance of inoculated *aip10-1* plants. ABAP1 and its
832 interacting proteins (AIP) negatively regulate DNA replication by reducing the activity of the
833 pre-replication complex (preRC) and by decreasing transcription of preRC members as
834 *AtCdt1a* and *AtCdt1b* (Masuda *et al.*, 2008). *AtABAP1* overexpression reduces DNA
835 replication and cell division rates in *A. thaliana*, whereas reduced *AtABAP1* expression leads
836 to higher cell division rates and enhanced plant growth (Masuda *et al.*, 2008). Recently,
837 (Montessoro *et al.*, 2025) described a combined role of AIP10 and ABAP1 as negative
838 modulators of proliferative cell divisions in all plant meristems, by direct interaction between
839 them. In addition, *ABAP1* expression was reduced in *aip10-1* plants suggesting that AIP10 may
840 also control cell division through a feedback mechanism of *ABAP1* transcriptional control. Our
841 results suggest that the enhanced growth of *aip10-1* plants in response to bioinoculants can be

842 increased by the negative regulation of *ABAP1*, favoring higher cell division rates and increased
843 growth. Moreover, *AtCDT1a* showed increased expression in *aip10-1* plants after inoculation
844 with both bioinoculants. A similar pattern was observed for the cell division marker *CYCB1;1*,
845 supporting the idea that beneficial bacterial colonization could stimulate the higher cell division
846 rates observed in *aip10-1*.

847 Nutrient availability decisively modulated the interaction between PGPB and *aip10-1*
848 plants, with an intensified growth-promoting response under low-fertilization conditions.
849 Nitrogen levels in the environment regulate the expression of multiple genes involved in
850 assimilation, transport, and utilization (Wilkinson and Crawford, 1993; Lothier *et al.*, 2011;
851 O'Brien *et al.*, 2016). In this study, we investigated the regulation of genes associated with
852 nitrogen assimilation which are modulated by variations in N sources, especially when
853 combined with the presence of PGPB (Rosman *et al.*, 2024).

854 Inoculation with *H. seropedicae* promoted the induction of *NIA1* in plants lacking
855 *AIP10* grown under low-nitrogen fertilization conditions. In plants, nitrate absorbed by the
856 roots is reduced to ammonium by nitrate reductase, encoded by *NIA1* and *NIA2*, and
857 subsequently incorporated into amino acids (Wilkinson and Crawford, 1993). Transcriptome
858 analysis revealed that *NIA1* was induced in shoots and roots of *A. thaliana* in response to
859 inoculation with Pal5, at 50 DAI (Soares *et al.*, 2024). Moreover, inoculation with the
860 endophytic fungus *Piriformospora indica* leads to the induction of NR gene expression,
861 resulting in increased nitrogen accumulation in Arabidopsis and tobacco seedlings (Sherameti
862 *et al.*, 2005). Ammonium is primarily assimilated in the roots, from where it travels to the aerial
863 parts of the plant, initially being converted into glutamine through an ATP-dependent reaction
864 catalyzed by GS (Tobin and Yamaya, 2001; Thomsen *et al.*, 2014). The expression dynamics
865 of *GLN1;1*, which encodes for a high-affinity ammonium isoform, have shown that regardless
866 of nutrient availability conditions, mutant plants tend to exhibit higher expression levels. In
867 response to inoculation with HRC54 and Pal5, this tendency is markedly more pronounced
868 under low-nutrient conditions. Given that *GLN1;1* and *GLN1;4* are highly expressed under low
869 nitrogen availability, studies presume that high-affinity isoforms play a predominant role in
870 ammonium assimilation at low concentrations in roots (Lothier *et al.*, 2011; Konishi *et al.*,
871 2018). Notably, high N availability induced the expression of *NIA1*, *NIA2*, and *GLN1;3,* which
872 can contribute to ammonium assimilation under conditions of sufficient ammonium
873 availability, in non-inoculated mutant plants compared to wild-type plants, with no additional
874 effect of inoculation. These results align with findings from (Montessoro *et al.*, 2025) showing
875 that *AIP10* mutants achieve superior carbon assimilation and biomass gain under high

876 fertilization. In an integrated manner, the results suggest that silencing *AIP10* favors the
877 induction of ammonium assimilation pathways, mainly in roots submitted to high nitrogen
878 levels. However, under conditions of low availability, this pattern was only reproduced in
879 inoculated mutants, particularly those inoculated with HRC54. From a bacterial perspective,
880 *nifH* expression in HRC54 and PAL5 associated with plant roots was quantified at 7 DAI,
881 before differential fertilization, and at 16 DAI, after three days of nutritional treatment. *aip10-*
882 *1* plants consistently showed higher *nifH* levels than Col-0 for both strains at 7 DAI.
883 Remarkably, this difference persisted at 16 DAI only under low-nutrient conditions. Given that
884 the plant growth-promoting capacity of *H. seropedicae* and *G. diazotrophicus* is associated
885 with the coordinated action of genes linked to N_2 fixation (Pedrosa *et al.*, 2011; Tufail *et al.*,
886 2021), our results suggest that the loss of function of AIP10 not only increases root colonization
887 but also potentiates bacterial N_2-fixation metabolism, especially in environments with low N
888 availability.
889

890 **AIP10 as a key regulatory target for improving plant performance under nutrient-limited**
891 **conditions in association with PGPB**

892 Conventional strategies for maintaining high crop productivity largely depend on the
893 extensive application of nitrogen-based fertilizers. However, crop yields have not increased
894 proportionally to fertilizer inputs, revealing low NUE and higher production costs (Mueller *et*
895 *al.*, 2019). In this context, to meet the nutritional needs of crops and maintain high levels of
896 productivity, modern agriculture has resorted to the use of bio-inputs, which favor plant
897 production, soil health, and the reduction of GHG emissions. Therefore, investing in
898 alternatives such as modulation of native root microbiomes to favor enrichment with PGPB, or
899 development PGPB-based biological inputs, becomes crucial strategies to ensure the
900 agricultural sustainability of various crops such as maize, sugarcane, wheat, and rice (Canellas
901 *et al.*, 2013; Martins *et al.*, 2020; Carril *et al.*, 2021; Pankievicz *et al.*, 2021; Tufail *et al.*, 2021).
902 Dissecting the plant genetic factors that govern the attraction of beneficial PGPB within the
903 microbiome, as well as the establishment of effective interactions with PGPB-based
904 bioinoculants, is essential for improving crop yield and plant fitness.
905 The absence of AIP10 shaped root microbiome to a higher abundance of PGPB and
906 diazotrophic bacteria. This technology also increased responsiveness to colonization by
907 bioinoculants under low nutrient availability. Remarkably, the enhanced traits observed in non-

908 inoculated *aip10-1* plants were further amplified upon inoculation, indicating additive effects
909 on plant growth promotion. PGPB inoculation in low nutrient availability resulted in enhanced
910 growth similar to that observed in non-inoculated mutant plants grown under high fertilization
911 (Montessoro *et al.*, 2025). Under these conditions, inoculation increased shoot biomass
912 accumulation by up to 35% in *aip10-1* plants under low fertilization. Regarding root
913 development, silencing *AIP10* promoted the formation of more robust root systems in response
914 to inoculation with HRC54 and Pal5 under low fertilization, increasing root surface area by up
915 to 42% compared to Col-0. This enhanced root growth resulted in a significant increase in dry
916 biomass, with gains of up to 70% after inoculation, equivalent to the increase observed in non-
917 inoculated *aip10-1* plants grown under high fertilization. The efficiency of the interaction
918 between plants and PGPB has been widely attributed to external conditions, including plant
919 genotype, bacterial genotype, and soil nutrient availability (Ballesteros *et al.*, 2021; Carvalho
920 *et al.*, 2022; Rosman *et al.*, 2024). Among these factors, the nutritional composition of the soil
921 stands out, playing an essential role in controlling plant growth and development, including the
922 establishment of the plant-PGPB association. Low nitrogen fertilization conditions encourage
923 the establishment of efficient plant-bacteria associations (Tufail *et al.*, 2021; Rosman *et al.*,
924 2024). In sugarcane, the association with PGPB can contribute up to 70% of all accumulated
925 N through BNF or improved NUE, varying according to the plant and bacterial genotype and
926 soil fertility (Urquiaga *et al.*, 2012; Antunes *et al.*, 2019; Martins *et al.*, 2020; Singh *et al.*,
927 2021). Among the diazotrophic bacteria that are associated with sugarcane, the *Herbaspirillum*
928 stands out, found colonizing the apoplast of leaves, very close to the vascular parenchyma cells
929 (Silva *et al.*, 2003). Several studies have already reported the positive effects of this association,
930 such as promoting increased biomass, shoot and secondary root growth, as well as the
931 accumulation of N, P and K (Oliveira *et al.*, 2006; dos Santos *et al.*, 2020; Martins *et al.*, 2020).
932 Specifically for *H. seropedicae* in maize, inoculation has been shown to increase root fresh
933 mass, root surface area (Nunes *et al.*, 2021); number of lateral roots (Do Amaral *et al.*, 2014;
934 Ferrari *et al.*, 2014; Hardoim *et al.*, 2020); N accumulation (Brusamarello-Santos *et al.*, 2017);
935 in addition to altering N metabolism and ensuring tolerance to abiotic stresses (Alves *et al.*,
936 2014; Curá *et al.*, 2017; Breda *et al.*, 2019; Dias *et al.*, 2021). Moreover, *aip10-1* plants
937 inoculated with Biofree showed increased rosette expansion and biomass accumulation
938 compared with mock-treated mutants under low nutrient availability. As this commercial
939 bioinoculant comprises *A. brasilense* Ab-V6 and *P. fluorescens* CCTB03, PGPB associated
940 with phytohormone synthesis and phosphate solubilization (Park *et al.*, 2009; Zhao *et al.*,
941 2025), these results suggest that multiple growth-promoting mechanisms may contribute to

942 enhanced plant performance in plants with silenced *AIP10* expression under reduced chemical
943 fertilization.

944 Our observations raise the important question of why the loss of AIP10 function, a gene
945 conserved across terrestrial plants, confer advantages such as enhanced root colonization by
946 beneficial bacteria. We previously proposed that AIP10 acts within an integrated regulatory
947 network that maintains transcriptional homeostasis among its components, to fine-tune plant
948 responses to environmental conditions. Several traits displayed by the loss of AIP10 activity
949 are associated with improved resilience linked to the conquest of the terrestrial environment,
950 including higher CO_2 assimilation and reduced transpiration, leading to more efficient water
951 use. We can hypothesize that AIP10 function on soil-microbe interactions have also evolved
952 in the context of plant adaptation to terrestrial environments.

953 Enhancing plant-beneficial bacteria interactions, either in native microbiome or in
954 response to inoculation, emerges as a strategic alternative to increase agricultural productivity
955 and advance towards sustainable practices. Here, we investigated the modulation of the native
956 root microbiome and the response to inoculation with bioinoculants of *A. thaliana aip10-1*
957 plants with silenced *AIP10* expression, aiming to increase plant growth and biomass
958 accumulation in scenarios of lower chemical fertilizer use. Remarkably, under low fertilization
959 conditions, plants lacking AIP10 shaped their root microbiome to a higher abundance of PGPB
960 and diazotrophic bacteria. *aip10-1* mutants also respond better to bioinoculants, under low
961 fertilization conditions, accumulating biomass comparable to that of non-inoculated mutants
962 grown with high fertilization. In addition, similarly to the vegetative phase, low fertilization
963 increased reproductive development, leading to a 29% increase in siliques on the main
964 inflorescence axis compared with all other groups under the same conditions. Taken together,
965 our results indicate that modifying *AIP10* expression, previously associated with the control of
966 a central hub that integrates cell division rates and primary metabolism, can be used as a
967 strategy to improve nutrient use efficiency under low chemical fertilization, contributing for a
968 more sustainable and regenerative agriculture. This approach results in a real increase in
969 biomass, productivity, and possibly the nutritional value of the plants, having an important
970 impact on food security.

971 **Supplementary data**

972 The following supplementary data are available at JWB online.

973 Supplementary Table S1. Primers used in this study.

974 Supplementary Table S2. Relative abundance of diazotrophic, plant growth–promoting
975 (PGPB), and pathogenic bacterial communities associated with the roots of Col-0 and *aip10-1*
976 plants.

977 Supplementary Fig. S1. Differential gene expression patterns in roots Col-0 and *aip10-1* of *A.*
978 *thaliana* 11 days after germination.

979 Supplementary Fig S2. Visualization of bacterial colonization patterns in different root zones
980 of *A. thaliana* Col-0 and *aip10-1* mutant plants.

981 Supplementary Fig S3. Experimental design of the differential fertilization trial in *aip10-1* and
982 wild-type Col-0 plants inoculated with *H. seropedicae* HRC54 (HRC54), *G. diazotrophicus*
983 Pal5 (Pal5), Biofree or non-inoculated (mock).

984 Supplementary Fig S4. Growth performance and physiological responses of Col-0 and *aip10-*
985 *1* plants inoculated with commercial bioinoculant Biofree under contrasting nutrient
986 conditions.

987 Supplementary Fig S5. Root architecture responses of Col-0 and *aip10-1 A. thaliana* plants to
988 Biofree inoculation under contrasting nutrient conditions.

989 Supplementary Fig S6. Reproductive performance of Col-0 and *aip10-1 A. thaliana* plants in
990 response to Biofree inoculation under high- and low-nutrient conditions.

991 **Author contribution**

992 MCU: Data curation, Investigation, Methodology, Writing – original draft, Writing – review
993 & editing. HF: Data curation, Investigation, Methodology, Writing – original draft, Writing –
994 review & editing. PM: Data curation, Methodology, Writing – original draft. JVS:
995 Methodology, Writing – original draft. SGE: Data curation, Methodology, AH: Funding
996 acquisition, Supervision, Writing – review & editing.

997 **Conflict of interest**

998 The authors declare that there is no conflict of interest.

999 **Funding**

This research was supported by grants from Fundação de Amparo a Pesquisa do Estado do Rio de Janeiro (FAPERJ) and Conselho Nacional de Desenvolvimento Científico e Tecnológico (CNPq). CNPq, FAPERJ, and the Coordination for the Improvement of Higher Education Personnel (CAPES) also supported the work with graduate and post-graduate scholarships. MCU and HF were supported by a CNPq postdoctoral fellowship. PM were supported by CNPq/SEMPI/MCTI grant no. 021/2021 (Rhae Program). SGE was supported by a CAPES MSc fellowship. JVS was supported by a CNPq undergraduate fellowship. ASH was supported by a research scientist fellowship from CNPq (306643/2022-7).

5. References

Alves GC, Videira SS, Urquiaga S, Reis VM. 2014. Differential plant growth promotion and nitrogen fixation in two genotypes of maize by several Herbaspirillum inoculants. Plant Soil, 1–15.

Do Amaral FP, Bueno JCF, Hermes VS, Arisi ACM. 2014. Gene expression analysis of maize seedlings (DKB240 variety) inoculated with plant growth promoting bacterium Herbaspirillum seropedicae. Symbiosis **62**, 41–50.

Antunes JEL, De Freitas ADS, Oliveira LMS, De Lyra MDCCP, Fonseca MAC, Santos CERS, De Oliveira JP, De Araújo ASF, Figueiredo MVB. 2019. Sugarcane inoculated with endophytic diazotrophic bacteria: Effects on yield, biological nitrogen fixation and industrial characteristics. Anais da Academia Brasileira de Ciencias **91**, 1–12.

Aquino JPA, Antunes JEL, Bonifácio A, Rocha SMB, Amorim MR, Alcântara Neto F, Araujo ASF. 2021. Plant growth-promoting bacteria improve growth and nitrogen metabolism in maize and sorghum. Theoretical and Experimental Plant Physiology **33**, 249–260.

Baldani JI, Pot B, Kirchhof G, *et al.* 1996. Emended Description of Herbaspirillum; Inclusion of [Pseudomonas] rubrisubalbicans, a Mild Plant Pathogen, as Herbaspirillum rubrisubalbicans comb. nov.; and Classification of a Group of Clinical Isolates (EF Group 1) as Herbaspirillum Species 3. International Journal of Systematic Bacteriology, 802–810.

Ballesteros HGF, Rosman AC, Carvalho TLG, Grativol C, Hemerly AS. 2021. Cell wall formation pathways are differentially regulated in sugarcane contrasting genotypes associated with endophytic diazotrophic bacteria. Planta **254**, 1–21.

Bauhus J, Messier C. 1999. IMAGE ANALYSIS Evaluation of Fine Root Length and Diameter Measurements Obtained Using RHIZO Image Analysis. Agronomie **91**, 142–147.

Breda FA, da Silva TFR, dos Santos SG, Alves GC, Reis VM. 2019. Modulation of nitrogen metabolism of maize plants inoculated with Azospirillum brasilense and Herbaspirillum seropedicae. Archives of Microbiology **201**, 547–558.

Brusamarello-Santos LC, Gilard F, Brulé L, Quilleré I, Gourion B, Ratet P, De Souza EM, Lea PJ, Hirel B. 2017. Metabolic profiling of two maize (Zea mays L.) inbred lines inoculated with the nitrogen fixing plant-interacting bacteria Herbaspirillum seropedicae and Azospirillum brasilense. PLoS ONE **12**, 1–19.

1040 **Canellas LP, Balmori DM, Médici LO, Aguiar NO, Campostrini E, Rosa RCC, Façanha**
1041 **AR, Olivares FL**. 2013. A combination of humic substances and Herbaspirillum seropedicae
1042 inoculation enhances the growth of maize (Zea mays L.). Plant and Soil **366**, 119–132.
1043 **Carneiro AK, Montessoro P da F, Fusaro AF, Araújo BG, Hemerly AS**. 2021. Plant
1044 cdks—driving the cell cycle through climate change. Plants **10**, 1–27.
1045 **Carril P, Cruz J, di Serio C, Pieraccini G, Ait Bessai S, Tenreiro R, Cruz C**. 2021.
1046 Modulation of the Wheat Seed-Borne Bacterial Community by Herbaspirillum seropedicae
1047 RAM10 and Its Potential Effects for Tryptophan Metabolism in the Root Endosphere.
1048 Frontiers in Microbiology **12**.
1049 **Carvalho T, Ballesteros H, Thiebaut F, Ferreira P, Hemerly A**. 2016. Nice to meet you:
1050 genetic, epigenetic and metabolic controls of plant perception of beneficial associative and
1051 endophytic diazotrophic bacteria in non-leguminous plants. Plant Molecular Biology **90**, 1–
1052 14.
1053 **Carvalho TLG, Balsemão-Pires E, Saraiva RM, Ferreira PCG, Hemerly AS**. 2014.
1054 Nitrogen signalling in plant interactions with associative and endophytic diazotrophic
1055 bacteria. Journal of Experimental Botany **65**, 5631–5642.
1056 **Carvalho TLG, Ferreira PCG, Hemerly AS**. 2011. Sugarcane Genetic Controls Involved
1057 in the Association with Beneficial Endophytic Nitrogen Fixing Bacteria. Tropical Plant
1058 Biology **4**, 31–41.
1059 **Carvalho TLG, Rosman AC, Grativol C, Nogueira EM, Baldani J, Hemerly AS**. 2022.
1060 Sugarcane Genotypes with Contrasting Biological Nitrogen Fixation Efficiencies
1061 Differentially Modulate Nitrogen. Plants **11**, 1–31.
1062 **Cohen AC, Bottini R, Pontin M, Berli FJ, Moreno D, Boccanlandro H, Travaglia CN,**
1063 **Piccoli PN**. 2015. Azospirillum brasilense ameliorates the response of Arabidopsis thaliana
1064 to drought mainly via enhancement of ABA levels. Physiologia Plantarum **153**, 79–90.
1065 **Curá A, Franz DR, Filosofía JE, Balestrasse KB, Burgueño LE**. 2017. Inoculation with
1066 Azospirillum sp . and Herbaspirillum sp . Bacteria Increases the Tolerance of Maize to
1067 Drought Stress. Microorganisms, 1–16.
1068 **Dias AC, Alves GC, Da Silva TFR, Alves BJR, Santos LA, Reis VM**. 2021. Comparison
1069 of N uptake of maize inoculated with two diazotrophic bacterial species grown under two N
1070 levels. Archives of Agronomy and Soil Science **00**, 1–17.
1071 **Dora S, Terrett OM, Sánchez-Rodríguez C**. 2022. Plant-microbe interactions in the
1072 apoplast: Communication at the plant cell wall. Plant Cell **34**, 1532–1550.
1073 **Doyle JJ, Doyle JL**. 1987. A Rapid DNA Isolation Procedure for Small Quantities of Fresh
1074 Leaf Tissue. Phytochemical Bulletin **19**, 11–15.
1075 **Draeger C, Ndinyanka Fabrice T, Gineau E, *et al.*** 2015. Arabidopsis leucine-rich repeat
1076 extensin (LRX) proteins modify cell wall composition and influence plant growth. BMC
1077 Plant Biology **15**, 1–11.
1078 **Espindula E, Sperb ER, Bach E, Passaglia LMP**. 2019. The combined analysis as the best
1079 strategy for dual RNA-seq mapping. Genetics and Molecular Biology **42**.
1080 **Faus I, Niñoles R, Kesari V, Llabata P, Tam E, Nebauer SG, Santiago J, Hauser MT,**
1081 **Gadea J**. 2018. Arabidopsis ILITHYIA protein is necessary for proper chloroplast biogenesis
1082 and root development independent of eIF2α phosphorylation. Journal of Plant Physiology
1083 **224–225**, 173–182.

Favero VO, Carvalho RH, Motta VM, Leite ABC, Coelho MRR, Xavier GR, Rumjanek NG, Urquiaga S. 2021. Bradyrhizobium as the Only Rhizobial Inhabitant of Mung Bean (Vigna radiata) Nodules in Tropical Soils: A Strategy Based on Microbiome for Improving Biological Nitrogen Fixation Using Bio-Products. Frontiers in Plant Science **11**, 1–16.

Ferrarezi JA, Carvalho-Estrada P de A, Batista BD, *et al.* 2022. Effects of inoculation with plant growth-promoting rhizobacteria from the Brazilian Amazon on the bacterial community associated with maize in field. Applied Soil Ecology **170**, 1–14.

Ferrari CS, Amaral FP, Bueno JCF, Scariot MC, Valentim-Neto PA, Arisi ACM. 2014. Expressed Proteins of Herbaspirillum seropedicae in Maize (DKB240) Roots-Bacteria Interaction Revealed Using Proteomics. Applied Biochemistry and Biotechnology **174**, 2267–2277.

Filgueiras L, Silva R, Almeida I, Vidal M, Baldani JI, Meneses CHSG. 2020. Gluconacetobacter diazotrophicus mitigates drought stress in Oryza sativa L. Plant and Soil **451**, 57–73.

Fukami J, Ollero FJ, Megías M, Hungria M. 2017. Phytohormones and induction of plant-stress tolerance and defense genes by seed and foliar inoculation with Azospirillum brasilense cells and metabolites promote maize growth. AMB Express **7**, 1–13.

Gao Y, Feng J, Wu J, Wang K, Wu S, Liu H, Jiang M. 2022. Transcriptome analysis of the growth-promoting effect of volatile organic compounds produced by Microbacterium aurantiacum GX14001 on tobacco (Nicotiana benthamiana). BMC Plant Biology **22**, 1–15.

Govindasamy P, Muthusamy SK, Bagavathiannan M, *et al.* 2023. Nitrogen use efficiency—a key to enhance crop productivity under a changing climate. Frontiers in Plant Science **14**, 1–48.

Harbort CJ, Hashimoto M, Inoue H, *et al.* 2020. Root-Secreted Coumarins and the Microbiota Interact to Improve Iron Nutrition in Arabidopsis. Cell Host and Microbe **28**, 825-837.e6.

Hardoim PR, de Carvalho TLG, Ballesteros HGF, Bellieny-Rabelo D, Rojas CA, Venancio TM, Ferreira PCG, Hemerly AS. 2020. Genome-wide transcriptome profiling provides insights into the responses of maize (Zea mays L.) to diazotrophic bacteria. Plant and Soil **451**, 121–143.

Hemelda NM, Noutoshi Y. 2025. Root-exuded sugars as drivers of rhizosphere microbiome assembly. Plant Biotechnology **42**, 215–227.

Huang AC, Jiang T, Liu YX, Bai YC, Reed J, Qu B, Goossens A, Nützmann HW, Bai Y, Osbourn A. 2019. A specialized metabolic network selectively modulates Arabidopsis root microbiota. Science **364**, 1–11.

Ishiyama K, Inoue E, Watanabe-Takahashi A, Obara M, Yamaya T, Takahashi H. 2004. Kinetic Properties and Ammonium-dependent Regulation of Cytosolic Isoenzymes of Glutamine Synthetase in Arabidopsis. Journal of Biological Chemistry **279**, 16598–16605.

Jones AR, Forero-Vargas M, Withers SP, Smith RS, Traas J, Dewitte W, Murray JAH. 2017. Cell-size dependent progression of the cell cycle creates homeostasis and flexibility of plant cell size. Nature Communications **8**, 1–13.

Jorgensen P, Tyers M. 2004. How cells coordinate growth and division. Current Biology **14**, 1–14.

Kandel SL, Joubert PM, Doty SL. 2017. Bacterial endophyte colonization and distribution within plants. Microorganisms **5**.

Konishi N, Saito M, Imagawa F, Kanno K, Yamaya T, Kojima S. 2018. Cytosolic Glutamine Synthetase Isozymes Play Redundant Roles in Ammonium Assimilation under Low-Ammonium Conditions in Roots of Arabidopsis thaliana. Plant and Cell Physiology **59**, 601–613.

Leandro MR, Rangel PL, dos Santos TC, *et al.* 2019. Colonization of Arabidopsis thaliana by Herbaspirillum seropedicae promotes its growth and changes its proteomic profile. Plant and Soil **443**, 429–447.

Lebeis SL, Sur Herrera Paredes, Derek S. Lundberg, *et al.* 2015. Salicylic acid modulates colonizationof the root microbiome by specificbacterial taxa. Science **349**, 860–864.

Liu H, Carvalhais LC, Crawford M, Singh E, Dennis PG, Pieterse CMJ, Schenk PM. 2017. Inner plant values: Diversity, colonization and benefits from endophytic bacteria. Frontiers in Microbiology **8**, 1–17.

Liu Y, Xu C, Chen S, Chu G, Yu K, Wang D. 2025. Beyond genotype: the influence of developmental stage on rice rhizospheric microbiome-metabolome networks. BMC Plant Biology **25**.

Logemann J, Schell J, Willmitzer L. 1987. Improved Method for the Isolation of RNA from Plant Tissues. ANALYTICAL BIOCHEMISTRY **163**, 16–20.

Lothier J, Gaufichon L, Sormani R, Lemaître T, Azzopardi M, Morin H, Chardon F, Reisdorf-Cren M, Avice JC, Masclaux-Daubresse C. 2011. The cytosolic glutamine synthetase GLN1;2 plays a role in the control of plant growth and ammonium homeostasis in Arabidopsis rosettes when nitrate supply is not limiting. Journal of Experimental Botany **62**, 1375–1390.

Ma KW, Niu Y, Jia Y, *et al.* 2021. Coordination of microbe–host homeostasis by crosstalk with plant innate immunity. Nature Plants **7**, 814–825.

Martins DS, Reis VM, Schultz N, Alves BJR, Urquiaga S, Pereira W, Sousa JS, Boddey RM. 2020. Both the contribution of soil nitrogen and of biological N2 fixation to sugarcane can increase with the inoculation of diazotrophic bacteria. Plant and Soil **454**, 155–169.

Masuda HP, Cabral LM, De Veylder L, Tanurdzic M, De Almeida Engler J, Geelen D, Inzé D, Martienssen RA, Ferreira PCG, Hemerly AS. 2008. ABAP1 is a novel plant Armadillo BTB protein involved in DNA replication and transcription. EMBO Journal **27**, 2746–2756.

Monaghan J, Li X. 2010. The HEAT repeat protein ILITYHIA is Required for plant immunity. Plant and Cell Physiology **51**, 742–753.

Montessoro P, Paixão JFR, Costa CNM, *et al.* 2025. The ABAP1 interacting protein 10 (AIP10) exerts a dual role in the cell cycle and primary metabolism pathways in Arabidopis thaliana. Plant Journal **123**, 1–24.

Moretti LG, Crusciol CAC, Bossolani JW, Calonego JC, Moreira A, Garcia A, Momesso L, Kuramae EE, Hungria M. 2021. Beneficial microbial species and metabolites alleviate soybean oxidative damage and increase grain yield during short dry spells. European Journal of Agronomy **127**, 1–12.

Mueller SM, Messina CD, Vyn TJ. 2019. Simultaneous gains in grain yield and nitrogen efficiency over 70 years of maize genetic improvement. Scientific Reports **9**, 1–8.

Nichio BT de L, Chaves RBR, Pedrosa F de O, Raittz RT. 2025. Exploring diazotrophic diversity: unveiling Nif core distribution and evolutionary patterns in nitrogen-fixing organisms. BMC Genomics **26**, 1–17.

Nunes R de O, Domiciano Abrahão G, de Sousa Alves W, Aparecida de Oliveira J, César Sousa Nogueira F, Pasqualoto Canellas L, Lopes Olivares F, Benedeta Zingali R, Soares MR. 2021. Quantitative proteomic analysis reveals altered enzyme expression profile in Zea mays roots during the early stages of colonization by Herbaspirillum seropedicae. Proteomics **21**, 1–12.

O'Brien JAA, Vega A, Bouguyon E, Krouk G, Gojon A, Coruzzi G, Gutiérrez RAA. 2016. Nitrate Transport, Sensing, and Responses in Plants. Molecular Plant **9**, 837–856.

Oliveira LM De, Canuto EDL, Urquiaga S, Reis VM. 2006. Yield of micropropagated sugarcane varieties in different soil types following inoculation with diazotrophic bacteria. **1**, 23–32.

Omara P, Aula L, Oyebiyi F, Raun WR. 2019. World Cereal Nitrogen Use Efficiency Trends: Review and Current Knowledge. Agrosystems, Geosciences and Environment **2**, 1–8.

Orozco-Mosqueda M del C, Santoyo G, Glick BR. 2023. Recent Advances in the Bacterial Phytohormone Modulation of Plant Growth. Plants **12**, 1–15.

Pankievicz VC, do Amaral FP, Ané JM, Stacey G. 2021. Diazotrophic bacteria and their mechanisms to interact and benefit cereals. Molecular Plant-Microbe Interactions **34**, 491–498.

Park KH, Lee CY, Son HJ. 2009. Mechanism of insoluble phosphate solubilization by Pseudomonas fluorescens RAF15 isolated from ginseng rhizosphere and its plant growth-promoting activities. Letters in Applied Microbiology **49**, 222–228.

Pedrosa FO, Monteiro RA, Wassem R, *et al.* 2011. Genome of herbaspirillum seropedicae strain SmR1, a specialized diazotrophic endophyte of tropical grasses. PLoS Genetics **7**, 1–10.

Pereira W, Oliveira RP, Pereira A, Sousa JS, Schultz N, Urquiaga S, Reis VM. 2021. Nitrogen acquisition and 15N-fertiliser recovery efficiency of sugarcane cultivar RB92579 inoculated with five diazotrophs. Nutrient Cycling in Agroecosystems **119**, 37–50.

Pierik R, Fankhauser C, Strader LC, Sinha N. 2021. Architecture and plasticity: Optimizing plant performance in dynamic environments. Plant Physiology **187**, 1029–1032.

Qi F, Zhang F. 2020. Cell cycle regulation in the plant response to stress. Frontiers in Plant Science **10**, 1–23.

Rodrigues GL, Matteoli FP, Gazara RK, *et al.* 2022. Characterization of cellular, biochemical and genomic features of the diazotrophic plant growth-promoting bacterium Azospirillum sp. UENF-412522, a novel member of the Azospirillum genus. Microbiological Research **254**, 1–12.

Rosman AC, Urquiaga MC de O, Thiebaut F, Ballesteros HGF, de Oliveira EAG, Hemerly AS. 2024. Dual RNA-seq of maize and H. seropedicae ZAE94 association, in different doses of nitrate, reveals novel insights into Plant-PGPB-environment relationship. Frontiers in Plant Science **15**, 1–23.

Di Salvo LP, Cellucci GC, Carlino ME, García de Salamone IE. 2018. Plant growth-promoting rhizobacteria inoculation and nitrogen fertilization increase maize (Zea mays L.)

grain yield and modified rhizosphere microbial communities. Applied Soil Ecology **126**, 113–120.

dos Santos R, Andrea P, Diaz E, Lana L, Lobo B. 2020. Use of Plant Growth-Promoting Rhizobacteria in Maize and Sugarcane : Characteristics and Applications. **4**, 1–15.

Dos Santos TC, Leandro MR, Maia CY, Rangel P, Soares FS, Reis R, Passamani L, Silveira V, De Souza Filho GA. 2020. Arabidopsis thaliana exudates induce growth and proteomic changes in Gluconacetobacter diazotrophicus. PeerJ **8**.

Schindelin J, Arganda-Carreras I, Frise E, *et al.* 2012. Fiji: An open-source platform for biological-image analysis. Nature Methods **9**, 676–682.

Sherameti I, Shahollari B, Venus Y, Altschmied L, Varma A, Oelmüller R. 2005. The endophytic fungus Piriformospora indica stimulates the expression of nitrate reductase and the starch-degrading enzyme glucan-water dikinase in tobacco and Arabidopsis roots through a homeodomain transcription factor that binds to a conserved motif in their promoters. Journal of Biological Chemistry **280**, 26241–26247.

Silva GL, Miguens CF, Olivares FL. 2003. Herbaspirillum seropedicae and sugarcane endophytic interaction investigated by using high pressure freezing electron microscopy. Brazilian Journal of Microbiology **34**, 69–71.

Singh P, Singh RK, Li HB, *et al.* 2021. Diazotrophic Bacteria Pantoea dispersa and Enterobacter asburiae Promote Sugarcane Growth by Inducing Nitrogen Uptake and Defense-Related Gene Expression. Frontiers in Microbiology **11**, 1–20.

Soares FS, Rangel de Souza ALS, de Souza SA, de Souza Vespoli L, Pinto VB, Matiello L, da Silva FR, Menossi M, de Souza Filho GA. 2024. Fine-Tuning of Arabidopsis thaliana Response to Endophytic Colonization by Gluconacetobacter diazotrophicus PAL5 Revealed by Transcriptomic Analysis. Plants **13**, 1–19.

Souza ALSR De, Souza SA De, Oliveira MVV De, Ferraz TM. 2016. Endophytic colonization of Arabidopsis thaliana by Gluconacetobacter diazotrophicus and its effect on plant growth promotion , plant physiology , and activation of plant defense. Plant Soil **399**, 257–270.

Srivastava S, Ranjan M, Bano N, Asif MH, Srivastava S. 2023. Comparative transcriptome analysis reveals the phosphate starvation alleviation mechanism of phosphate accumulating Pseudomonas putida in Arabidopsis thaliana. Scientific Reports **13**, 1–15.

Stringlis IA, Proietti S, Hickman R, Van Verk MC, Zamioudis C, Pieterse CMJ. 2018. Root transcriptional dynamics induced by beneficial rhizobacteria and microbial immune elicitors reveal signatures of adaptation to mutualists. Plant Journal **93**, 166–180.

Tang J, Wu D, Li X, *et al.* 2022. Plant immunity suppression via PHR1-RALF-FERONIA shapes the root microbiome to alleviate phosphate starvation. The EMBO Journal **41**, 1–19.

Thiebaut F, Rojas CA, Grativol C, *et al.* 2017. Roles of non-coding RNA in sugarcane-microbe interaction. Non-coding RNA **3**, 1–24.

Thiebaut F, Urquiaga MC de O, Rosman AC, da Silva ML, Hemerly AS. 2022. The Impact of Non-Nodulating Diazotrophic Bacteria in Agriculture: Understanding the Molecular Mechanisms That Benefit Crops. International Journal of Molecular Sciences **23**, 1–22.

Thomsen HC, Eriksson D, Møller IS, Schjoerring JK. 2014. Cytosolic glutamine synthetase: A target for improvement of crop nitrogen use efficiency? Trends in Plant Science **19**, 656–663.

Tian W, Li L, Xiao X, *et al.* 2022. Identification of a plant endophytic growth-promoting bacteria capable of inhibiting cadmium uptake in rice. Journal of Applied Microbiology **132**, 520–531.

Tilman D, Balzer C, Hill J, Befort BL. 2011. Global food demand and the sustainable intensification of agriculture. Proceedings of the National Academy of Sciences of the United States of America **108**, 20260–20264.

Tobin AK, Yamaya T. 2001. Cellular compartmentation of ammonium assimilation in rice and barley. Journal of Experimental Botany **52**, 591–604.

Tufail MA, Touceda-González M, Pertot I, Ehlers RU. 2021. Gluconacetobacter diazotrophicus pal5 enhances plant robustness status under the combination of moderate drought and low nitrogen stress in zea mays l. Microorganisms **9**.

Upadhyay SK, Srivastava AK, Rajput VD, Chauhan PK, Bhojiya AA, Jain D, Chaubey G, Dwivedi P, Sharma B, Minkina T. 2022. Root Exudates: Mechanistic Insight of Plant Growth Promoting Rhizobacteria for Sustainable Crop Production. Frontiers in Microbiology **13**.

Urquiaga S, Boddey R. 1992. Contribution of Nitrogen Fixation to Sugar Cane: Nitrogen15 and NitrogenBalance Estimates. doi: 10.2136/sssaj1992.03615995005600010017x.

Urquiaga S, Xavier RP, de Morais RF, *et al.* 2012. Evidence from field nitrogen balance and 15N natural abundance data for the contribution of biological N 2 fixation to Brazilian sugarcane varieties. Plant and Soil **356**, 5–21.

Vacheron J, Desbrosses G, Bouffaud ML, Touraine B, Moënne-Loccoz Y, Muller D, Legendre L, Wisniewski-Dyé F, Prigent-Combaret C. 2013. Plant growth-promoting rhizobacteria and root system functioning. Frontiers in Plant Science **4**, 1–19.

Vandenkoornhuyse P, Quaiser A, Duhamel M, Le Van A, Dufresne A. 2015. The importance of the microbiome of the plant holobiont. New Phytologist **206**, 1196–1206.

Vargas L, Brígida A, Mota J, *et al.* 2014. Drought tolerance conferred to sugarcane by association with Gluconacetobacter diazotrophicus: A transcriptomic view of hormone pathways. PLoS ONE, 1–37.

Vargas L, de Carvalho TLG, Ferreira PCG, Baldani VLD, Baldani JI, Hemerly AS. 2012. Early responses of rice (Oryza sativa L.) seedlings to inoculation with beneficial diazotrophic bacteria are dependent on plant and bacterial genotypes. Plant and Soil **356**, 127–137.

Voges MJEEE, Bai Y, Schulze-Lefert P, Sattely ES. 2019. Plant-derived coumarins shape the composition of an Arabidopsis synthetic root microbiome. Proceedings of the National Academy of Sciences of the United States of America **116**, 12558–12565.

Wilkinson JQ, Crawford NM. 1993. Identification and characterization of a chlorate-resistant mutant of Arabidopsis thaliana with mutations in both nitrate reductase structural genes NIA1 and NIA2. Molecular Genetics and Genomics **239**, 289–297.

Zhang J, Liu W, Bu J, Lin Y, Bai Y. 2023. Host genetics regulate the plant microbiome. Current Opinion in Microbiology **72**.

1299 **Zhang J, Liu YX, Zhang N, *et al.*** 2019. NRT1.1B is associated with root microbiota
1300 composition and nitrogen use in field-grown rice. Nature Biotechnology **37**, 676–684.
1301 **Zhao H, Xu J, Huang L, Ding Y, Lin X, Sun C**. 2025. Auxin and Root Hair Defective Six-
1302 Like 4 Regulate Azospirillum brasilense-Induced Root Hair Development in Arabidopsis.
1303 Plant, Cell and Environment, 1–2.
1304 **Zluhan-Martínez E, López-Ruíz BA, García-Gómez ML, García-Ponce B, de la Paz**
1305 **Sánchez M, Álvarez-Buylla ER, Garay-Arroyo A**. 2021. Integrative Roles of
1306 Phytohormones on Cell Proliferation, Elongation and Differentiation in the Arabidopsis
1307 thaliana Primary Root. Frontiers in Plant Science **12**, 1–20.
1308 **Zuluaga MYA, Milani KML, Gonçalves LSA, De Oliveira ALM**. 2020. Diversity and
1309 plant growth-promoting functions of diazotrophic/N-scavenging bacteria isolated from the
1310 soils and rhizospheres of two species of Solanum. PLoS ONE **15**, 1–25.

1311

1312 **Table S1.** Primers used in this study.

Primer name	Primer Forward Sequence	Primer Reverse Sequence	Organism
RT-qPCR			
GAPDH	TTGGTGACAACAGGTCAAGCA	AAACTTGTCGCTCAATGCAATC	*A. thaliana*
UBI14	TCACTGGAAAGACCATTACTCTTGAA	AGCTGTTTTCCAGCGAAGATG	*A. thaliana*
ABAP1	TCAGCCTTAAGAAGAGCTTGCA	ACCATAATTGAGAGCTGAGCTTAGTG	*A. thaliana*
Cdt1a	AATCCGATCACGTCTTGAAGAAG	GAACCACGATCTCAAGAAAGCA	*A. thaliana*
Cyclin B1;1	CCTCCATTCACTCTCAACAG	CCTGGCAGCTGTGGAATATG	*A. thaliana*
ILA	CCCGACGGTTATCCAAGTTTC	ACATGTTTCCTCCTACCCACTTACA	*A. thaliana*
LRX4	CACTCCTCACGCAGATGTATCG	CTGACTTCGGTGTCGGAGAGA	*A. thaliana*
RSL4	TGGGATGGACATTGGTCTCA	CGTCCGAAGGCGGAGAATA	*A. thaliana*
XHT14	GCCTCCCCAAGGAGTGTAAAC	CAAGATGAAACAAAACGGAAAGAA	*A. thaliana*
nifH	AACAAGGCGCAGGAAATCTA	AAATGCCCTTGGAGATGTTG	*H. seropedicae*
nifH	GCGTCCGCCAGATCGTATT	CTGGGTGGACTGATCTGCAA	*G. diazotrophicus*
q-PCR			
AZO-2	GCGCGGAAGTCCTGAAT	GGTGGTCGATAACTCCATCG	*A. brasiliense*
FIC	CGCAAGGCAAACTCCAGATG	CAGGCACACGCATTCTCTTTC	*H. seropedicae*
GSH	CCTGGCTCGTCTACCTGATC	TGAGGCGGTGACTGACAA	*G. diazotrophicus*

1313

1314 ## 6. Figure legends

1315 **Fig 1. Repression of AIP10 expression by plant growth–promoting bacteria and**
1316 **conservation of its nuclear protein structure in Arabidopsis and sugarcane. (A)**
1317 Expression profile of the *AIP10* homolog in sugarcane root and shoot tissues of two BNF
1318 contrasting genotypes (SP70-1143, high BNF; Chunee, low BNF) from plants naturally
1319 colonized by bacteria (Stalk) and plants grown under bacteria-free conditions (BF). Expression
1320 values are shown as $\log_2$ fold change. **(B)** Predicted protein structures of *AIP10* putative

homologs encoded by two isoforms *AT1G80940.1* and *AT1G80940.3* from *A. thaliana*, and *Sspoon.04G0001710-3D* from *Saccharum spontaneum*. Protein domains were predicted using the SMART program. The scheme shows the nuclear localization signal (NLS), coiled-coil, and ribosomal L32e domains, suggesting a possible role related to nuclear regulation and protein interaction, potentially conserved between species. **(C)** Expression levels of *AIP10* in *A. thaliana Col-0* plants at 7 DAI after inoculation with two different PGPB strains, *G. diazotrophicus* and *H. seropedicae*.

Fig 2. Taxonomic distribution and enrichment patterns of key microbial functional groups in roots and bulk soil of Col-0 and *aip10-1* plants following inoculation. (A) Venn diagram showing shared and unique microbial species associated with roots and surrounding soil from Col-0 and *aip10-1* plants. **(B–D)** Relative abundance (left panels) and z-score heatmaps (right panels) for microbial groups with functional relevance to plant performance, including **(B)** diazotrophic species, **(C)** plant growth-promoting bacteria (PGPB), and **(D)** pathogenic species. Data are shown for root and soil compartments of Col-0 wild type and *aip10-1* plants. In the heat map, the color red represents higher abundance, and blue represents lower abundance, according to the z-score value.

Fig 3. Functional effect of AIP10 silencing on *A. thaliana* root colonization and association with diazotrophic PGPB strains *H. seropedicae* HRC54 and *G. diazotrophicus* Pal5. (A) Representative images of Col-0 and aip10-1 plants inoculated with G. diazotrophicus Pal5 or H. seropedicae HRC54 at 20 days after germination (DAG). Mock-inoculated plants served as controls. **(B–E)** Growth and developmental parameters of Col-0 and aip10-1 plants inoculated with H. seropedicae HRC54 or G. diazotrophicus Pal5. **(B)** Primary root length and **(C)** lateral root number measured at 15 DAG. **(D)** Dry weight of the shoots and **(E)** rosette area measured at 21 DAG. Data are presented as box plots showing median, interquartile range, and minimum/maximum values. **(F, G)** Absolute qPCR quantification of *H. seropedicae* HRC54 and *G. diazotrophicus* Pal5 colonization in roots of Col-0 and aip10-1 at 7 DAI, respectively. The data represent the number of bacterial cells per gram of root tissue, obtained by absolute qPCR quantification. **(H, I)** Relative expression of the *nifH* gene in *H. seropedicae* HRC54 and *G. diazotrophicus* Pal5 colonizing Col-0 and aip10-1 roots at 7 DAI, quantified by RT-qPCR. Gene expression values are shown as fold-change relative to GAPDH and UBI14 reference genes and normalized to the mock-inoculated condition. **(J)** Confocal microscopy images showing colonization patterns of *G. diazotrophicus* (RFP-labeled) *H. seropedicae* (GFP-labeled) and in Col-0 and aip10-1 roots at 11 DAG and 7 DAI. Images include RFP, GFP, DIC, and merged channels. Statistical analyses were performed using Student's t-test at a 5% significance level. (*) indicates statistically significant differences ($p \leq 0.05$).

Fig 4. RT-qPCR analysis for genes involved in cell division, cell wall organization, bacterial response, and root morphogenesis in *aip10-1* and wild-type Col-0 roots, at 7 after inoculation. (A) *ABAP1*. **(B)** *CDT1a*. **(C)** *CYCB1;1*. **(D)** *LRX4*. **(E)** *ILA*. **(F)** *RSL4*. RT-qPCR results are presented as the ratio of expression of each gene relative to the constitutive expression of *GAPDH* and *UBI14* reference genes when compared to mock and inoculated plants. Bars represent mean ± standard deviation of the relative mRNA expression in three biological replicates and each biological replicate analyzed with three technical replicates. Statistical analysis was performed using the Student's t-test ($P \leq 0.05$). Means with different letters are significantly different at 5% level of confidence.

1368
1369 **Fig 5. Differential fertilization assay (0.06 g/L and 0.12 g/L NPK) on *aip10-1* and wild-**
1370 **type Col-0 plants inoculated with distinct plant growth-promotion bacteria. (A)**
1371 Representative images of *A. thaliana* Col-0 and *aip10-1* plants inoculated with *H. seropedicae*
1372 HRC54 at 35 DAG (31 DAI), grown in a greenhouse under two different fertilization
1373 conditions. **(B)** Representative images of *A. thaliana* Col-0 and *aip10-1* plants inoculated with
1374 *G. diazotrophicus* Pal5 at 35 DAG (31 DAI), grown in a greenhouse under two different
1375 fertilization conditions. **(C)** Rosette area measurement using ImageJ program in mock and
1376 HRC54-inoculated plants at 35 DAG. **(D)** Shoot dry weight in mock and HRC54-inoculated
1377 plants at 35 DAG. **(E)** Total chlorophyll content in leaf disks of mock and HRC54-inoculated
1378 plants at 35 DAG. **(F)** Rosette area measurement using ImageJ program in mock and Pal5-
1379 inoculated plants at 35 DAG. **(G)** Shoot dry weight in mock and Pal5-inoculated plants at 35
1380 DAG. **(H)** Total chlorophyll content in leaf disks of mock and Pal5-inoculated plants at 35
1381 DAG. The box plot graphs show the distribution of data of six individuals. The box represents
1382 the interquartile range (IQR), with the inner line running down the median. The whiskers
1383 extend to the maximum and minimum values, including all points within that range.
1384 Differences between groups were confirmed by Student's *t*-test and means followed by
1385 different letters indicate significant differences at the 5% confidence level.
1386
1387
1388 **Fig 6. Root development of Col-0 and *aip10-1* plants inoculated with different plant**
1389 **growth-promoting bacteria, grown in a greenhouse under two fertilization conditions at**
1390 **35 DAG. (A)** Root dry weight in mock and HRC54-inoculated plants. **(B)** Root length in mock
1391 and HRC54-inoculated plants. **(C)** Root surface area in mock and HRC54-inoculated plants.
1392 **(D)** Root dry weight in mock and Pal5-inoculated plants. **(E)** Root length in mock and Pal5-
1393 inoculated plants. **(F)** Root surface area in mock and Pal5-inoculated plants. The box plot
1394 graphs show the distribution of data of five individuals. The box represents the interquartile
1395 range (IQR), with the inner line running down the median. The whiskers extend to the
1396 maximum and minimum values, including all points within that range. Differences between
1397 groups were confirmed by Student's *t*-test and means followed by different letters indicate
1398 significant differences at the 5% confidence level.
1399
1400
1401 **Fig 7. Reproductive stage of Col-0 and *aip10-1* plants inoculated with different plant**
1402 **growth-promoting bacteria, cultivated in a greenhouse under two fertilization conditions**
1403 **at 60 DAG. (A)** Representative images of Col-0 and *aip10-1* during the reproductive stage
1404 compare the different responses to HRC54 and Pal5 inoculation, in response to low and high
1405 fertilization treatments. **(B)** Height of the main inflorescence axis in mock and HRC54-
1406 inoculated plants. **(C)** Total number of siliques in the main inflorescence axis in mock and
1407 HRC54-inoculated plants. **(D)** Total seed weight per individual in mock and HRC54-inoculated
1408 plants. **(E)** Height of the main inflorescence axis in mock and Pal5-inoculated plants. **(F)** Total
1409 number of siliques in the main inflorescence axis in mock and Pal5-inoculated plants. **(G)** Total
1410 seed weight per individual in mock and Pal5-inoculated plants. The box plot graphs show the
1411 distribution of data of five individuals. The box represents the interquartile range (IQR), with
1412 the inner line running down the median. The whiskers extend to the maximum and minimum
1413 values, including all points within that range. Differences between groups were confirmed by
1414 Student's *t*-test and means followed by different letters indicate significant differences at the
1415 5% confidence level.
1416

1417 **Figure 8. Expression profiling of nitrogen metabolism-related genes in Col-0 and *aip10-1***
1418 **roots, cultivated in a greenhouse under two fertilization conditions at 20 DAG.** Roots of
1419 wild-type Col-0 and the *aip10-1* knockout were cultivated in a greenhouse under high- and
1420 low-nitrogen fertilization and sampled at 20 DAG for RT-qPCR analysis.(**A, B**) GLN1;1
1421 transcript levels in mock-, *H. seropedicae* HRC54–, and *G. diazotrophicus* Pal5–inoculated
1422 plants.(**C, D**) GLN1;3 transcript levels across the same inoculation treatments.(**E, F**)
1423 Expression patterns of NIA1, and (**G, H**) NIA2, in mock-, HRC54-, and Pal5-inoculated
1424 roots.(I, J) *nifH* transcript abundance from *H. seropedicae* HRC54 and *G. diazotrophicus* Pal5
1425 colonizing Col-0 and *aip10-1* roots under both nitrogen treatments. Relative expression values
1426 were quantified by RT-qPCR and normalized by UBI14 and GAPDH reference genes. Data
1427 represent transcriptional responses to inoculation and nitrogen availability, highlighting
1428 genotype-dependent modulation of nitrogen assimilation pathways. Bars represent mean ±
1429 standard deviation of the relative mRNA expression in three biological replicates and each
1430 biological replicate analyzed with three technical replicates. Statistical analysis was performed
1431 using the Student's t-test ($P \leq 0.05$). Means with different letters are significantly different at
1432 5% level of confidence.
1433
1434 **Fig. 9. Expression profiling of nitrogen metabolism-related genes in Col-0 and *aip10-1***
1435 **roots of inoculated plants, cultivated in a greenhouse under two fertilization conditions at**
1436 **20 DAG.** Roots of wild-type Col-0 and the *aip10-1* knockout were cultivated in a greenhouse
1437 under high- and low-nitrogen fertilization and sampled at 20 DAG for RT-qPCR analysis. (**A,**
1438 **B**) *nifH* transcript abundance from *H. seropedicae* HRC54 and *G. diazotrophicus* Pal5
1439 colonizing Col-0 and *aip10-1* roots under both nitrogen treatments; **(B, C)** *GLN1;1* transcript
1440 levels in *H. seropedicae* HRC54–, *and G. diazotrophicu*s Pal5–inoculated plants; **(E, F)** *NIA1*
1441 transcript levels in *H. seropedicae* HRC54–, *and G. diazotrophicu*s Pal5–inoculated plants.
1442 Relative expression values were quantified by RT-qPCR and normalized by UBI14 and
1443 GAPDH reference genes. Bars represent mean ± standard deviation of the relative mRNA
1444 expression in three biological replicates and each biological replicate analyzed with three
1445 technical replicates. Statistical analysis was performed using the Student's t-test. Means with
1446 different letters are significantly different at 5% level of confidence.
1447
1448
1449 **Fig S1. Differential gene expression patterns in roots Col-0 and *aip10-1* of *A. thaliana* 11**
1450 **days after germination**. **(A)** Functional classification of differentially expressed transcripts
1451 (DEGs) in metabolic and biological pathways. **(B)** Gene expression pattern within the
1452 categories response to bacteria, hormone response, biotic stimulus response, and cell wall,
1453 highlighting the contribution of genes related to plant immunity and structural remodeling. **(C)**
1454 Expression pattern of genes involved in carbohydrate response, lipid metabolism, and general
1455 metabolic processes, suggesting an intense reorganization of energy and structural metabolism
1456 during root development. Expression values were obtained from RPKM data and represented
1457 as *log fold change* between *aip10-1*vs Col-0 roots. Pink bars indicate higher gene induction in
1458 *aip10-1*, while blue bars represent gene repression.

1459 **Fig S2. Visualization of bacterial colonization patterns in different root zones of *A.***
1460 ***thaliana* Col-0 and *aip10-1* mutant plants.** Confocal microscopy images showing bacterial
1461 localization in the meristematic zone, root hair area, elongation zone, and lateral root area.
1462 Plants were inoculated with *G. diazotrophicus* PAL5 strain expressing RFP (red) or *H.*
1463 *seropedicae* HRC54 strain expressing GFP (green) reporters, enabling direct visualization of
1464 colonization along the root surface and tissues. In *aip10-1* mutant roots, a higher fluorescence

signal was consistently observed across all analyzed regions, indicating a greater bacterial presence and colonization density compared with the Col-0 wild type. Scale bars = 100 µm.

Fig S3. Experimental design of the differential fertilization trial in *aip10-1* and wild-type Col-0 plants inoculated with *H. seropedicae* HRC54 (HRC54), *G. diazotrophicus* Pal5 (Pal5), Biofree or non-inoculated (mock). Seeds were pre-germinated *in vitro*, and seedlings were inoculated at 4 DAG. Seven days after inoculation (11 DAG), plants were transferred to the greenhouse. Differential irrigation treatments with low nutrients (0.06 g/L NPK; 20:20:20) and high nutrients (0.12 g/L NPK; 20:20:20) were initiated at 17 DAG. Samples for molecular analyses were collected at 11 and 20 DAG, while those for phenotypic analyses were collected at 35 and 60 DAG. Created with BioRender.com.

Fig S4. Growth performance and physiological responses of Col-0 and *aip10-1* plants inoculated with commercial bioinoculant Biofree under contrasting nutrient conditions. (A) Representative images of Col-0 and *aip10-1* plants grown under high-nutrient (HN) and low-nutrient (LN) conditions, and non-inoculated (Mock) or inoculated with the Biofree bacterial consortium. **(B)** Absolute qPCR quantification of *Azospirillum brasilense* Ab-V6 colonization in roots of Col-0 and aip10-1 at 7 DAI. **(C–E)** Quantification of key growth traits, including rosette area **(C)**, shoot dry weight **(B)**, and total chlorophyll content **(E)**. Plants were evaluated at the vegetative stage, and boxplots depict the distribution of five biological replicates. Different letters indicate statistically significant differences ($P \leq 0.05$).

Fig S5. Root architecture responses of Col-0 and *aip10-1 A. thaliana* plants to Biofree inoculation under contrasting nutrient conditions. (A) Representative root system images of Col-0 and *aip10-1* plants grown under high-nutrient and low-nutrient conditions, non-inoculated (Mock) or inoculated with the Biofree microbial consortium. Quantitative analysis of **(B)** root dry weight, **(C)** primary root length, and **(D)** total root surface area. Boxplots represent five biological replicates; different letters indicate statistically significant differences ($P \leq 0.05$).

Fig S6. Reproductive performance of Col-0 and *aip10-1 A. thaliana* plants in response to Biofree inoculation under high- and low-nutrient conditions. (A) Representative images of inflorescence Col-0 and *aip10-1* grown under high-fertility and low-fertility conditions, non-inoculated (Mock) or inoculated with the Biofree microbial consortium. **(B–D)** Quantification of reproductive traits including **(B)** main inflorescence length, **(C)** number of siliques per main inflorescence, and **(D)** total seed weight per plant. Data are presented as boxplots of five biological replicates; different letters denote significant differences ($P \leq 0.05$).

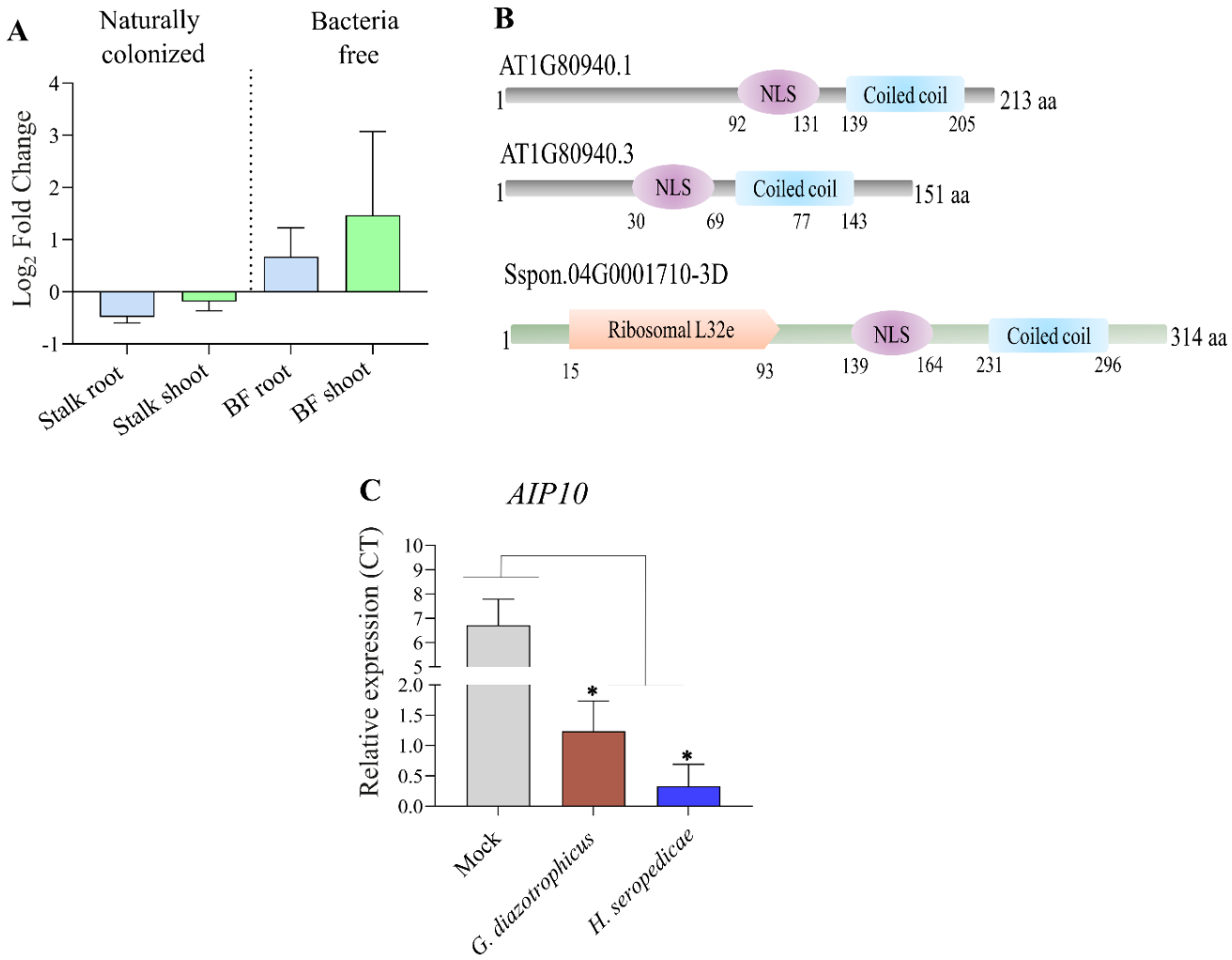

Fig 1. Repression of AIP10 expression by plant growth–promoting bacteria and conservation of its nuclear protein structure in Arabidopsis and sugarcane. (A) Expression profile of the *AIP10* homolog in sugarcane root and shoot tissues of two BNF contrasting genotypes (SP70-1143, high BNF; Chunee, low BNF) from plants naturally colonized by bacteria (Stalk) and plants grown under bacteria-free conditions (BF). Expression values are shown as $\log_2$ fold change. **(B)** Predicted protein structures of *AIP10* putative homologs encoded by two isoforms *AT1G80940.1* and *AT1G80940.3* from *A. thaliana*, and *Sspoon.04G0001710-3D* from *Saccharum spontaneum*. Protein domains were predicted using the SMART program. The scheme shows the nuclear localization signal (NLS), coiled-coil, and ribosomal L32e domains, suggesting a possible role related to nuclear regulation and protein interaction, potentially conserved between species. **(C)** Expression levels of *AIP10* in *A. thaliana Col-0* plants at 7 DAI after inoculation with two different PGPB strains, *G. diazotrophicus* and *H. seropedicae*.

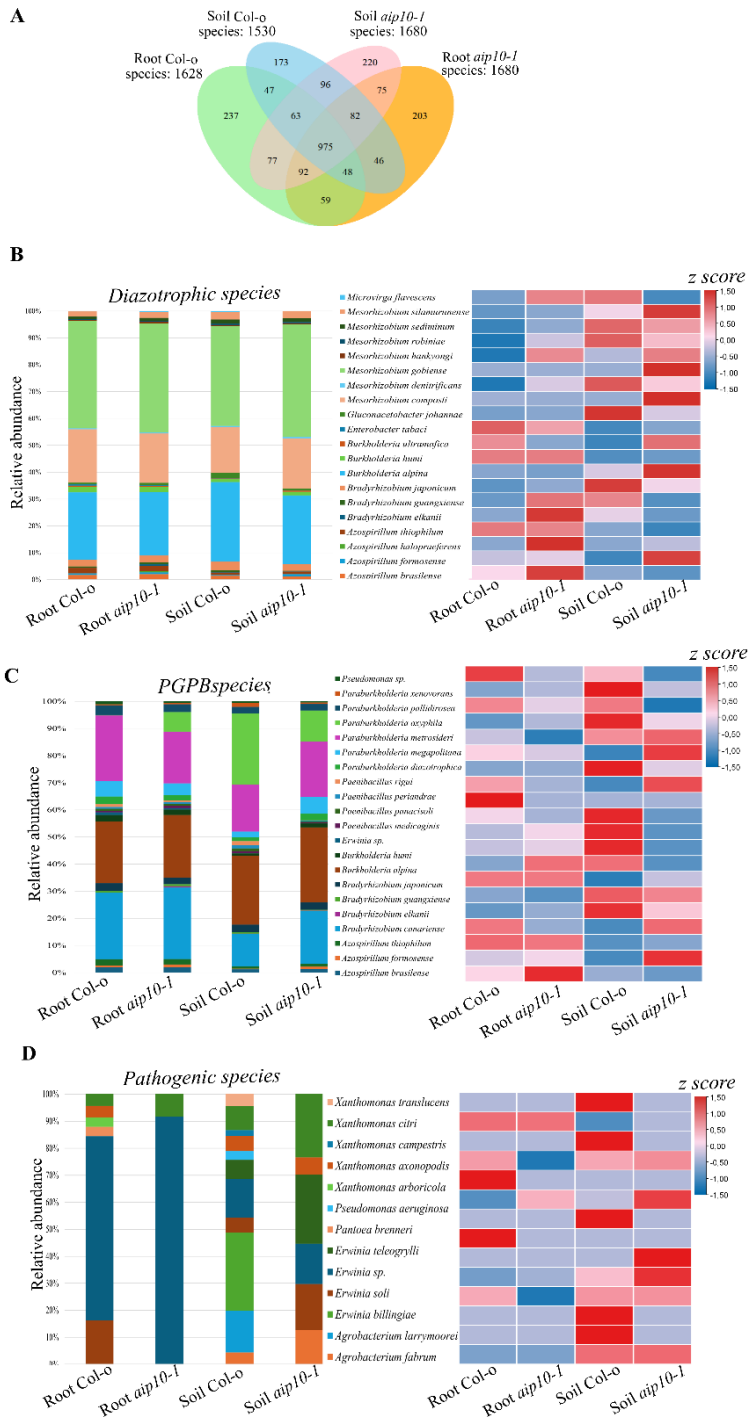

Fig 2. Taxonomic distribution and enrichment patterns of key microbial functional groups in roots and bulk soil of Col-0 and *aip10-1* plants following inoculation. (A) Venn diagram showing shared and unique microbial species associated with roots and surrounding soil from Col-0 and *aip10-1* plants. **(B–D)** Relative abundance (left panels) and z-score heatmaps (right panels) for microbial groups with functional relevance to plant performance, including **(B)** diazotrophic species, **(C)** plant growth-promoting bacteria (PGPB), and **(D)** pathogenic species. Data are shown for root and soil compartments of Col-0 wild type and *aip10-1* plants. In the heat map, the color red represents higher abundance, and blue represents lower abundance, according to the z-score value.

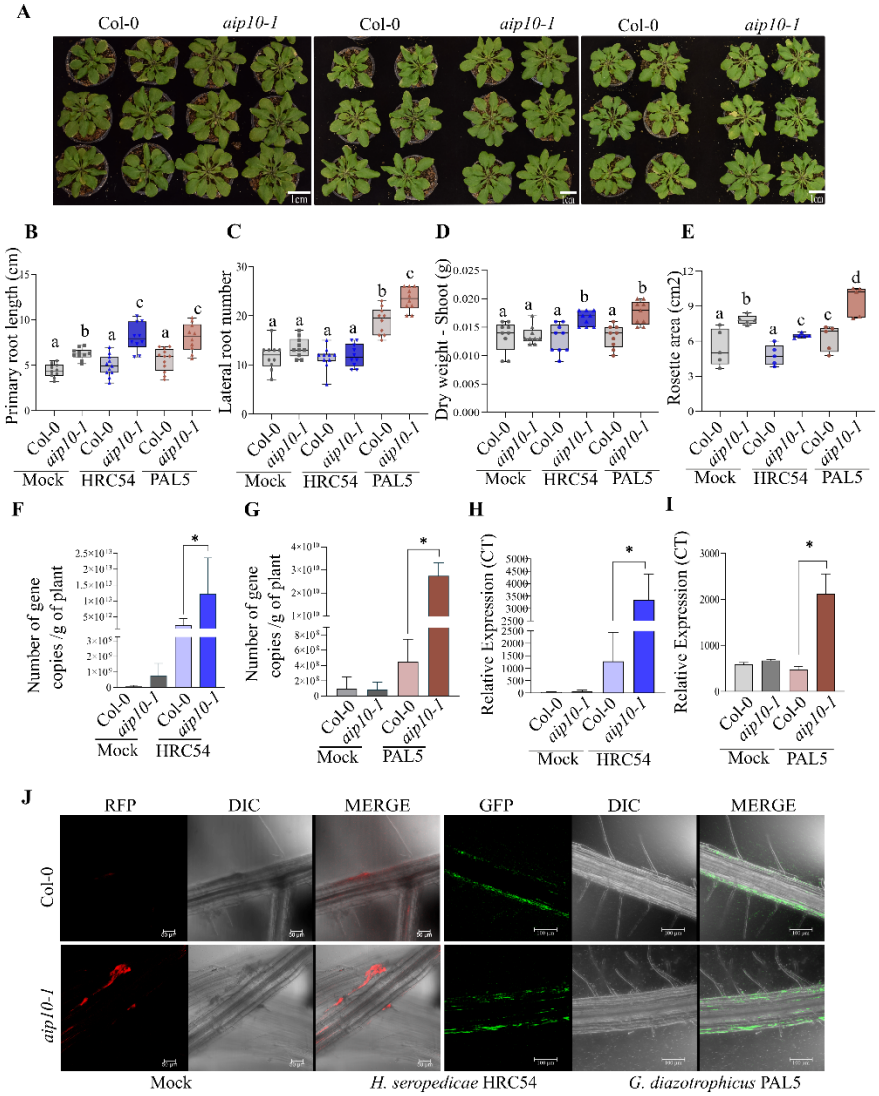

Fig 3. Functional effect of AIP10 silencing on *A. thaliana* root colonization and association with diazotrophic PGPB strains *H. seropedicae* HRC54 and *G. diazotrophicus* Pal5. (A) Representative images of Col-0 and aip10-1 plants inoculated with G. diazotrophicus Pal5 or H. seropedicae HRC54 at 20 days after germination (DAG). Mock-inoculated plants served as controls. **(B–E)** Growth and developmental parameters of Col-0 and aip10-1 plants inoculated with H. seropedicae HRC54 or G. diazotrophicus Pal5. **(B)** Primary root length and **(C)** lateral root number measured at 15 DAG. **(D)** Dry weight of the shoots and **(E)** rosette area measured at 21 DAG. Data are presented as box plots showing median, interquartile range, and minimum/maximum values. **(F, G)** Absolute qPCR quantification of *H. seropedicae* HRC54 and *G. diazotrophicus* Pal5 colonization in roots of Col-0 and aip10-1 at 7 DAI, respectively. The data represent the number of bacterial cells per gram of root tissue, obtained by absolute qPCR quantification. **(H, I)** Relative expression of the *nifH* gene in *H. seropedicae* HRC54 and *G. diazotrophicus* Pal5 colonizing Col-0 and aip10-1 roots at 7 DAI, quantified by RT-qPCR. Gene expression values are shown as fold-change relative to GAPDH and UBI14 reference genes and normalized to the mock-inoculated condition. **(J)** Confocal microscopy images showing colonization patterns of *G. diazotrophicus* (RFP-labeled) *H. seropedicae* (GFP-labeled) and in Col-0 and aip10-1 roots at 11 DAG and 7 DAI. Images include RFP, GFP, DIC, and merged channels. Statistical analyses were performed using Student's t-test at a 5% significance level. (*) indicates statistically significant differences ($p \leq 0.05$).

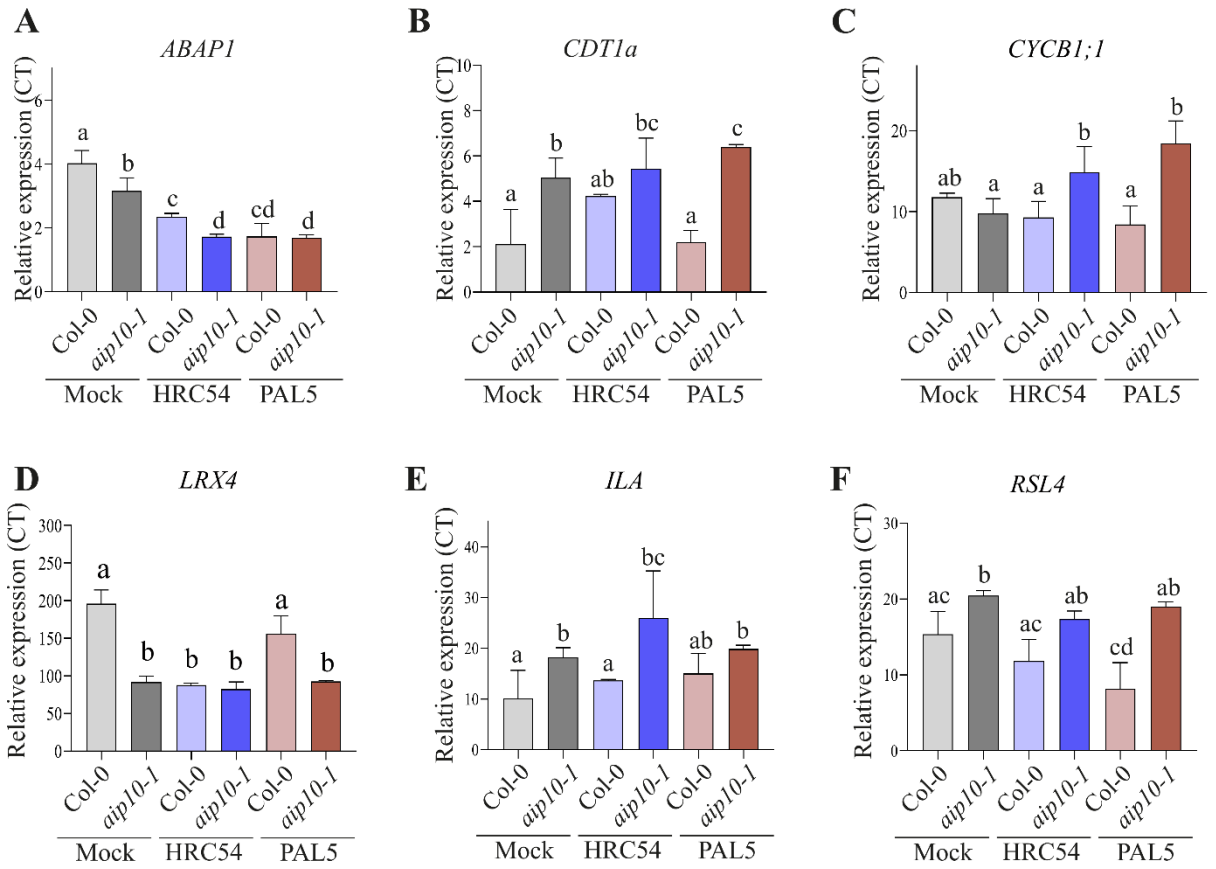

Fig 4. RT-qPCR analysis for genes involved in cell division, cell wall organization, bacterial response, and root morphogenesis in *aip10-1* and wild-type Col-0 roots, at 7 after inoculation. (A) *ABAP1*. **(B)** *CDT1a*. **(C)** *CYCB1;1*. **(D)** *LRX4*. **(E)** *ILA*. **(F)** *RSL4*. RT-qPCR results are presented as the ratio of expression of each gene relative to the constitutive expression of *GAPDH* and *UBI14* reference genes when compared to mock and inoculated plants. Bars represent mean ± standard deviation of the relative mRNA expression in three biological replicates and each biological replicate analyzed with three technical replicates. Statistical analysis was performed using the Student's t-test ($P \leq 0.05$). Means with different letters are significantly different at 5% level of confidence.

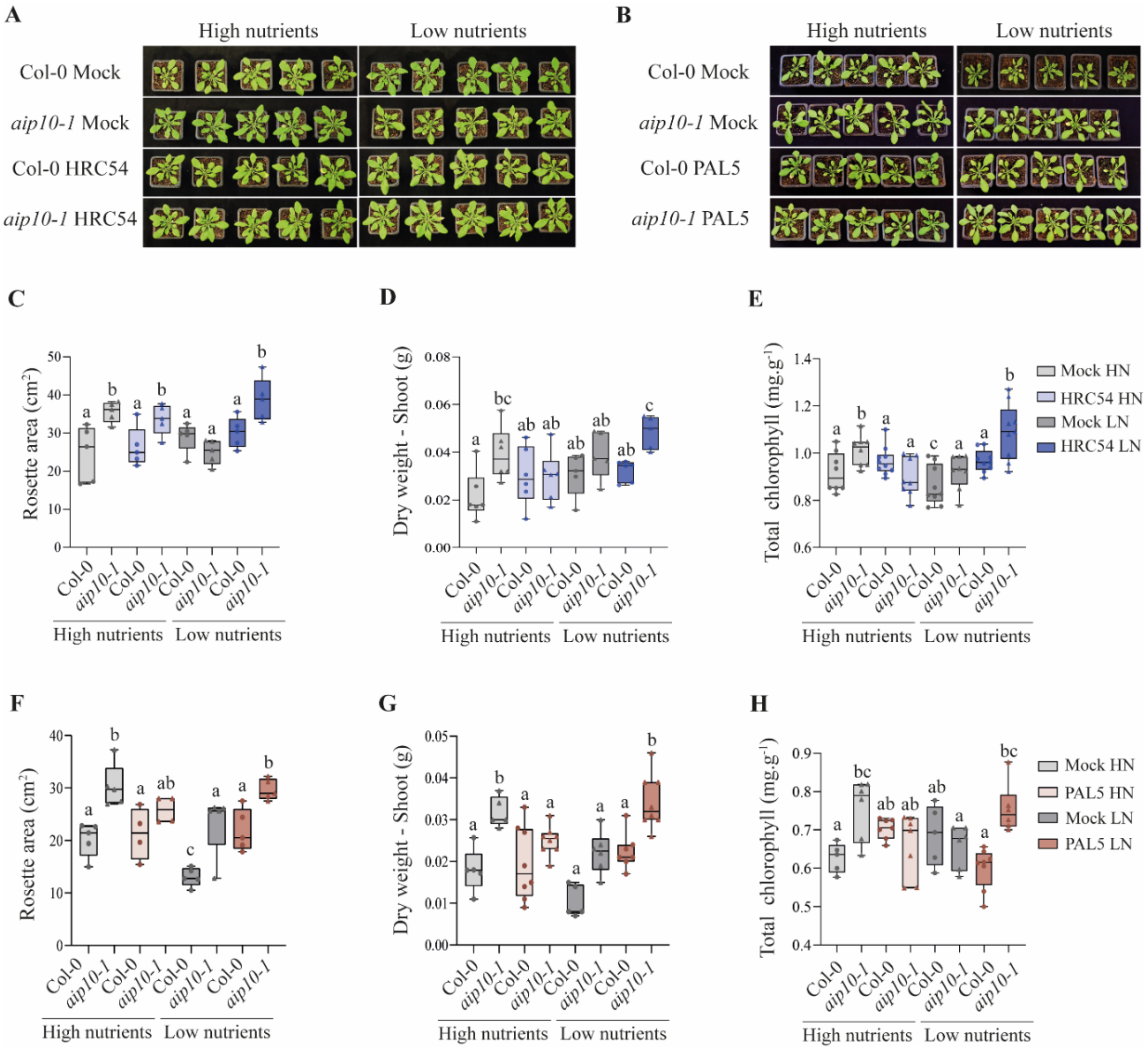

Fig 5. Differential fertilization assay (0.06 g/L and 0.12 g/L NPK) on *aip10-1* and wild-type Col-0 plants inoculated with distinct plant growth-promotion bacteria. (A) Representative images of *A. thaliana* Col-0 and *aip10-1* plants inoculated with *H. seropedicae* HRC54 at 35 DAG (31 DAI), grown in a greenhouse under two different fertilization conditions. **(B)** Representative images of *A. thaliana* Col-0 and *aip10-1* plants inoculated with *G. diazotrophicus* Pal5 at 35 DAG (31 DAI), grown in a greenhouse under two different fertilization conditions. **(C)** Rosette area measurement using ImageJ program in mock and HRC54-inoculated plants at 35 DAG. **(D)** Shoot dry weight in mock and HRC54-inoculated plants at 35 DAG. **(E)** Total chlorophyll content in leaf disks of mock and HRC54-inoculated plants at 35 DAG. **(F)** Rosette area measurement using ImageJ program in mock and Pal5-inoculated plants at 35 DAG. **(G)** Shoot dry weight in mock and Pal5-inoculated plants at 35 DAG. **(H)** Total chlorophyll content in leaf disks of mock and Pal5-inoculated plants at 35 DAG. The box plot graphs show the distribution of data of six individuals. The box represents the interquartile range (IQR), with the inner line running down the median. The whiskers extend to the maximum and minimum values, including all points within that range. Differences between groups were confirmed by Student's *t*-test and means followed by different letters indicate significant differences at the 5% confidence level.

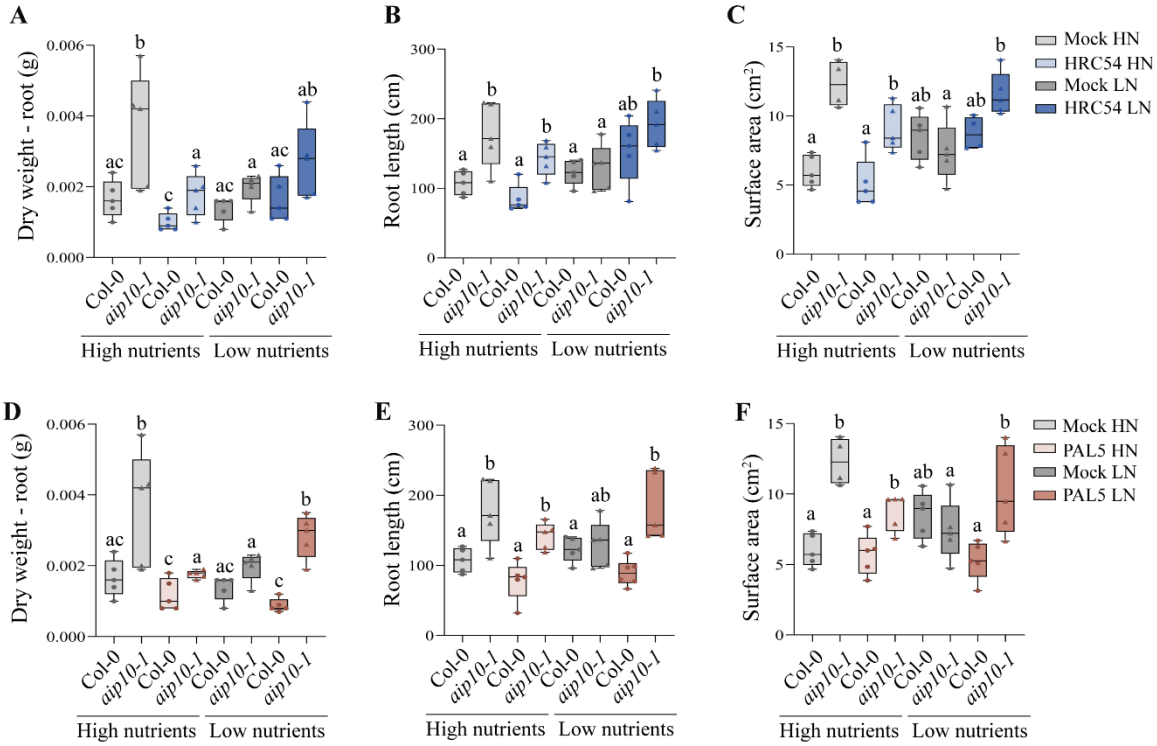

Fig 6. Root development of Col-0 and *aip10-1* plants inoculated with different plant growth-promoting bacteria, grown in a greenhouse under two fertilization conditions at 35 DAG. (A) Root dry weight in mock and HRC54-inoculated plants. **(B)** Root length in mock and HRC54-inoculated plants. **(C)** Root surface area in mock and HRC54-inoculated plants. **(D)** Root dry weight in mock and Pal5-inoculated plants. **(E)** Root length in mock and Pal5-inoculated plants. **(F)** Root surface area in mock and Pal5-inoculated plants. The box plot graphs show the distribution of data of five individuals. The box represents the interquartile range (IQR), with the inner line running down the median. The whiskers extend to the maximum and minimum values, including all points within that range. Differences between groups were confirmed by Student's *t*-test and means followed by different letters indicate significant differences at the 5% confidence level.

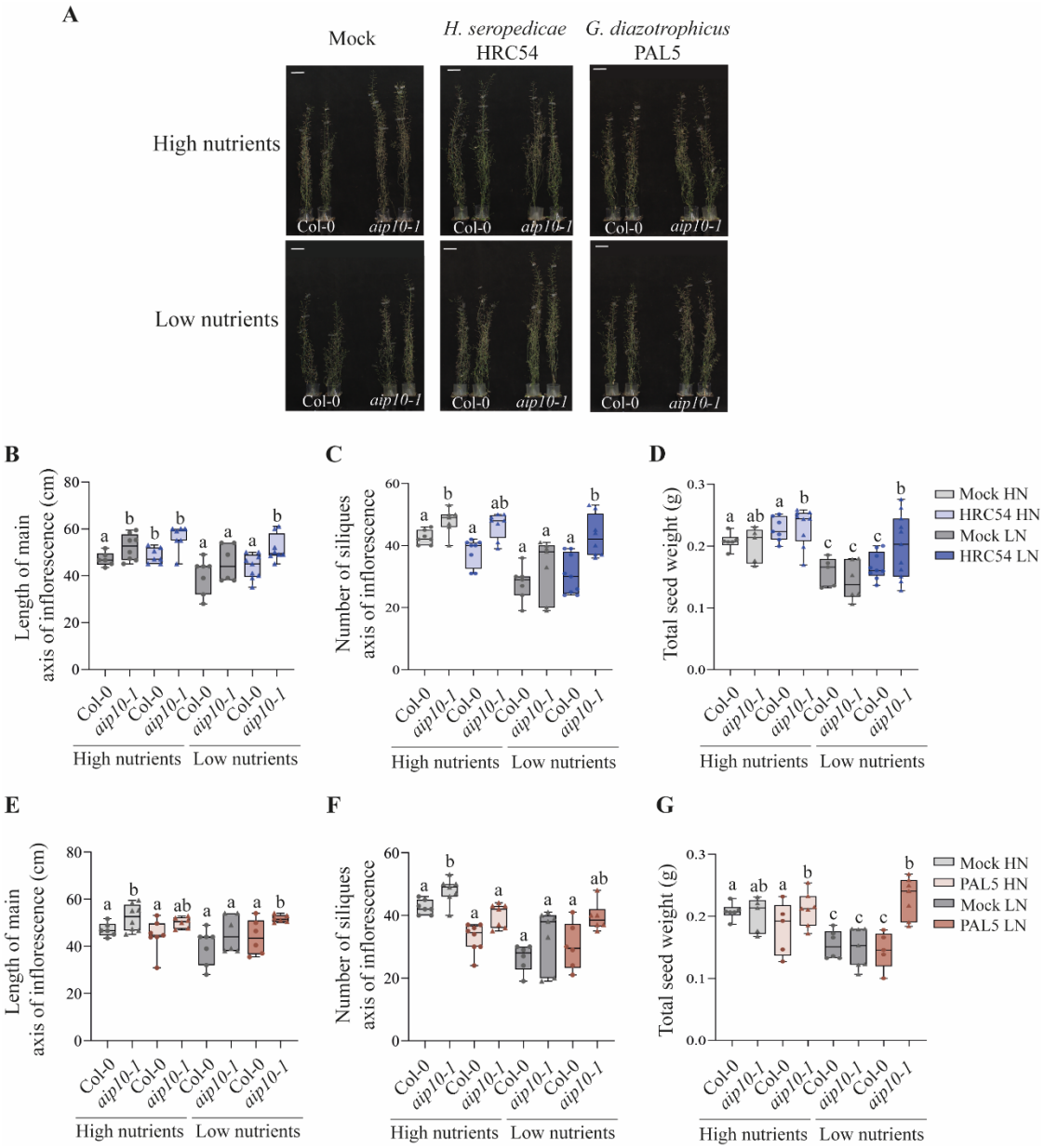

Fig 7. Reproductive stage of Col-0 and *aip10-1* plants inoculated with different plant growth-promoting bacteria, cultivated in a greenhouse under two fertilization conditions at 60 DAG. (A) Representative images of Col-0 and *aip10-1* during the reproductive stage compare the different responses to HRC54 and Pal5 inoculation, in response to low and high fertilization treatments. **(B)** Height of the main inflorescence axis in mock and HRC54-inoculated plants. **(C)** Total number of siliques in the main inflorescence axis in mock and HRC54-inoculated plants. **(D)** Total seed weight per individual in mock and HRC54-inoculated plants. **(E)** Height of the main inflorescence axis in mock and Pal5-inoculated plants. **(F)** Total number of siliques in the main inflorescence axis in mock and Pal5-inoculated plants. **(G)** Total seed weight per individual in mock and Pal5-inoculated plants. The box plot graphs show the distribution of data of five individuals. The box represents the interquartile range (IQR), with the inner line running down the median. The whiskers extend to the maximum and minimum values, including all points within that range. Differences between groups were confirmed by Student's *t*-test and means followed by different letters indicate significant differences at the 5% confidence level.

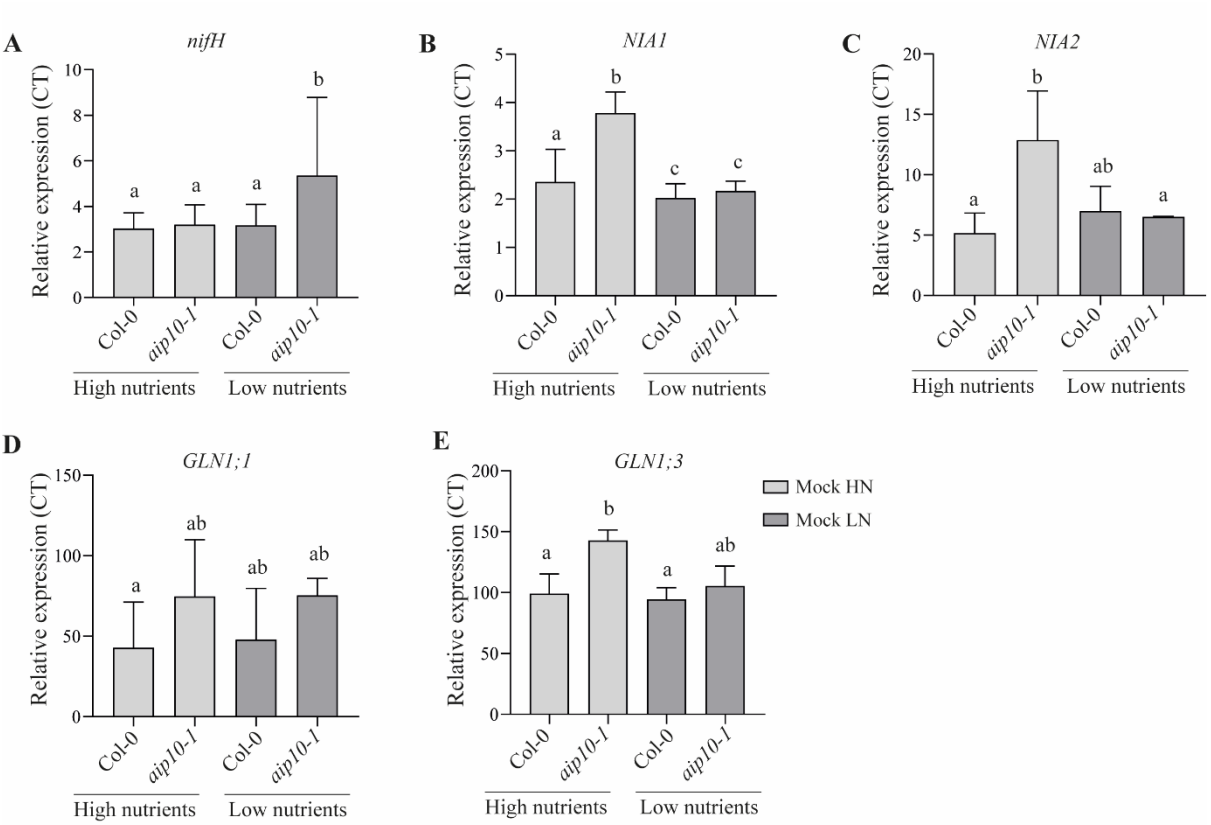

Figure 8. Expression profiling of nitrogen metabolism-related genes in Col-0 and *aip10-1* roots, cultivated in a greenhouse under two fertilization conditions at 20 DAG. Roots of wild-type Col-0 and the *aip10-1* knockout were cultivated in a greenhouse under high- and low-nitrogen fertilization and sampled at 20 DAG for RT-qPCR analysis.(**A, B**) GLN1;1 transcript levels in mock-, *H. seropedicae* HRC54–, and *G. diazotrophicus* Pal5–inoculated plants.(**C, D**) GLN1;3 transcript levels across the same inoculation treatments.(**E, F**) Expression patterns of NIA1, and (**G, H**) NIA2, in mock-, HRC54-, and Pal5-inoculated roots.(I, J) *nifH* transcript abundance from *H. seropedicae* HRC54 and *G. diazotrophicus* Pal5 colonizing Col-0 and *aip10-1* roots under both nitrogen treatments. Relative expression values were quantified by RT-qPCR and normalized by UBI14 and GAPDH reference genes. Data represent transcriptional responses to inoculation and nitrogen availability, highlighting genotype-dependent modulation of nitrogen assimilation pathways. Bars represent mean ± standard deviation of the relative mRNA expression in three biological replicates and each biological replicate analyzed with three technical replicates. Statistical analysis was performed using the Student's t-test ($P \leq 0.05$). Means with different letters are significantly different at 5% level of confidence.

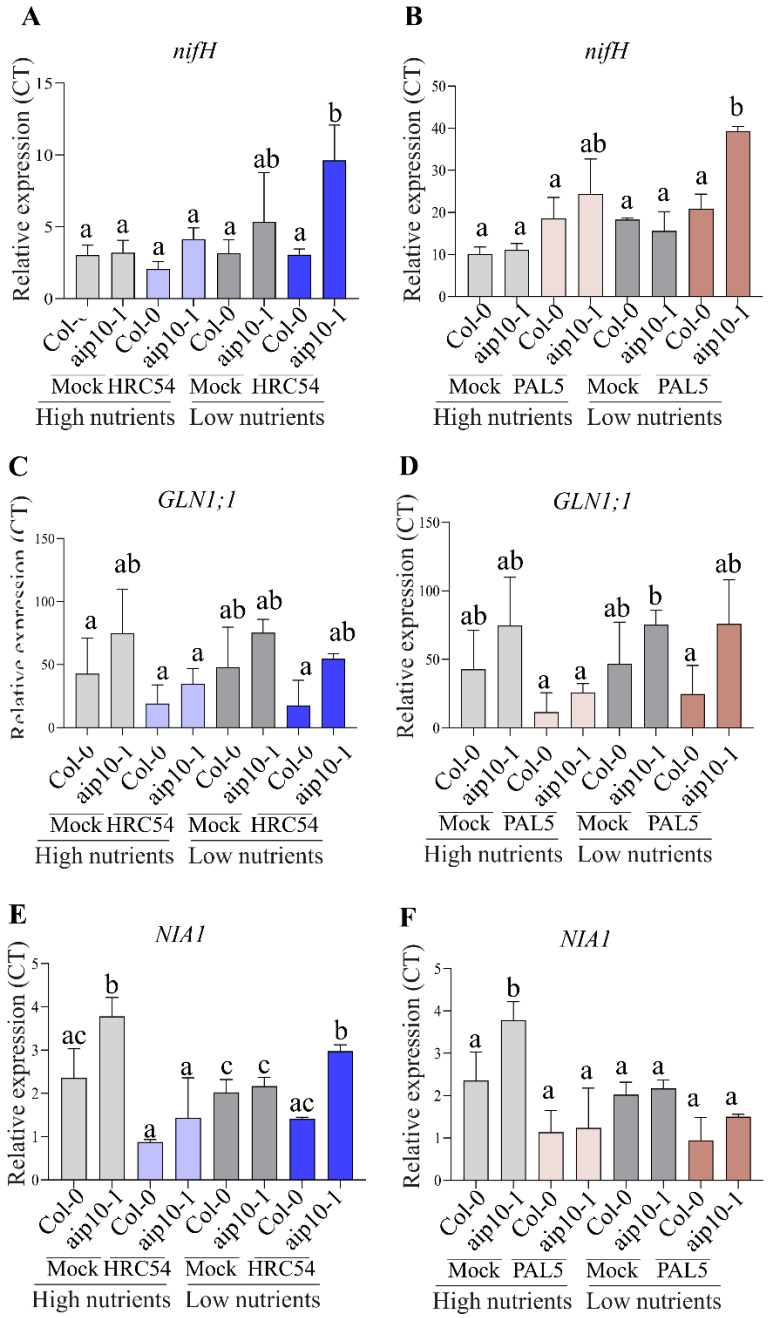

Fig. 9. Expression profiling of nitrogen metabolism-related genes in Col-0 and *aip10-1* roots of inoculated plants, cultivated in a greenhouse under two fertilization conditions at 20 DAG. Roots of wild-type Col-0 and the *aip10-1* knockout were cultivated in a greenhouse under high- and low-nitrogen fertilization and sampled at 20 DAG for RT-qPCR analysis. (**A, B**) *nifH* transcript abundance from *H. seropedicae* HRC54 and *G. diazotrophicus* Pal5 colonizing Col-0 and *aip10-1* roots under both nitrogen treatments; **(B, C)** *GLN1;1* transcript levels in *H. seropedicae* HRC54–, *and G. diazotrophicu*s Pal5–inoculated plants; **(E, F)** *NIA1* transcript levels in *H. seropedicae* HRC54–, *and G. diazotrophicu*s Pal5–inoculated plants. Relative expression values were quantified by RT-qPCR and normalized by UBI14 and GAPDH reference genes. Bars represent mean ± standard deviation of the relative mRNA expression in three biological replicates and each biological replicate analyzed with three technical replicates. Statistical analysis was performed using the Student's t-test. Means with different letters are significantly different at 5% level of confidence.